DLR Design Challenge 2024

Submitted on July 21, 2024

Participating Team

Clemens Ehrich
Luca Kriebel
Tim Schulz
Mathias Tekkel
Lennart Wauer
Leonid Wenz

Academic Advisors

Prof. Dr.-Ing. A. Bardenhagen
M.Sc. A. Richter

Team Members

Clemens Ehrich
M.Sc. Aerospace Engineering
4th Semester

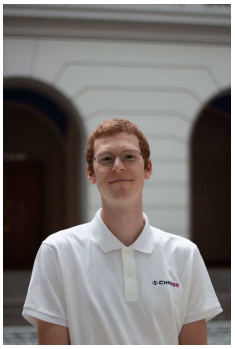

Luca Kriebel
M.Sc. Aerospace Engineering
2nd semester

Tim Schulz
M.Sc. Aerospace Engineering
1st Semester

Mathias Tekkel
M.Sc. Aerospace Engineering
4th semester

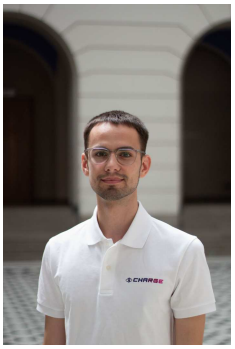

Lennart Wauer
B.Sc. Transportation Engineering
10th semester

Leonid Wenz
B.Sc. Transportation Engineering
10th Semester

Abstract

The aviation industry is a large emitter of greenhouse gases on a global scale. In recent years, the industry has begun to address the challenges of climate change, particularly in the context of domestic and short-haul operations, which have come under intense scrutiny for their significant greenhouse emissions, especially given the availability of climate friendly alternatives such as Europe's rail network. According to estimates, approximately 50 % of all flights starting from, or landing in Germany have been covering distances of less than 1,000 km [1]. The goal is to design a new regional aircraft concept that is both climate friendly but also cost effective with an expected entry into service until 2050. This demands a broad rethinking of energy sources, propulsion technology and alternative design concepts that deviate from the conventional wing-tube configuration. In order to identify the ideal design, various concepts are examined as well as different energy sources and propulsion systems. As a solution this paper proposes the narrow body, box wing aircraft-concept CHARGE. CHARGE is a battery electric aircraft with distributed electric propulsion. The aircraft is able to carry 110 passengers over a range of about 900 km, ideal for regional and domestic operation. To enhance operational efficiency and cost effectiveness CHARGE is equipped with integrated airstairs and an electric nose gear motor for airport independent operation, enable the aircraft to operate from small regional airports with minimal infrastructure. CHARGE is both energetically and economically superior to its reference aircraft on the given route network, making it a promising and viable concept.

Zusammenfassung

Die Luftfahrtindustrie ist weltweit einer der größten Verursacher von Treibhausgasemissionen. In den letzten Jahren hat die Luftfahrtindustrie begonnen, sich den Herausforderungen des Klimawandels zu stellen, insbesondere im Zusammenhang mit Inlands- und Kurzstreckenflügen, die aufgrund ihrer hohen Emissionen besonders kritisch betrachtet werden, vor allem angesichts der Verfügbarkeit umweltfreundlicherer Alternativen wie dem europäischen Schienennetz. Nach Angaben des Statistischen Bundesamtes sind 50 % aller Flüge, die an den deutschen Hauptverkehrsflughäfen starten oder landen, kürzer als 1.000 km. Ziel ist es, ein neues, klimafreundliches und wirtschaftliches Regionalflugzeugkonzept zu entwickeln, das bis 2050 in Dienst gestellt werden kann. Dies erfordert ein umfassendes Umdenken in Bezug auf Energiequellen, Antriebstechnologien und alternative Designkonzepte, die sich von der konventionellen Drachenkonfiguration unterscheiden. Um das ideale Design zu finden, werden verschiedene Konzepte sowie unterschiedliche Energiequellen und Antriebssysteme untersucht. Als Lösung präsentiert diese Arbeit das Schmalrumpf-Box-Wing-Flugzeug CHARGE. CHARGE ist ein rein batterieelektrisches Flugzeug mit verteiltem elektrischen Antrieb. Das Flugzeug kann 110 Passagiere über eine Reichweite von ca. 900 km befördern. Damit ist es ideal für Regional- und Inlandsflüge. Zur Steigerung der operationellen Effizienz und Kosteneffektivität ist CHARGE mit einer integrierten Fluggasttreppe und einem elektrischen Bugradmotor für den Einsatz unabhängig von Flughafeninfrastruktur ausgestattet, wodurch das Flugzeug von kleinen Regionalflughäfen mit minimaler Infrastruktur eingesetzt werden kann. CHARGE ist im Vergleich zum Referenzflugzeug auf dem angegebenen Streckennetz sowohl energetisch als auch wirtschaftlich überlegen und stellt ein vielversprechendes und zukunftfähiges Konzept dar.

Contents

List of Symbols

A	m^2	Area
a	°	Glide Angle
b	m	Wingspan
C_D	–	Drag Coefficient
C_L	–	Lift Coefficient
C'_L	–	Lift Gradient
c	–	Coefficient
c	°	Climb Angle
d	m	Diameter
D	N	Drag
e	–	Oswald Factor
ε	–	Geometric Wing Twist
η	–	Dimensionless Spanwise Coordinate
η	–	Efficiency
F	–	Factor
F	m^2	Area
φ	°	Wing Sweep
φ_{25}	°	Wing 25 % Line
G	N	Weight Force
γ	–	Dimensionless Circulation Distribution
h	m	Height, Horizontal Distance
i	–	Ratio
K	–	k-factor (“Grundrissfaktor”)
k	–	Pressure Drag Factor
l	m	Length or Depth
L	N	Lift
λ	–	Taper Ratio
Λ	–	Aspect Ratio
N	–	Number
m	kg	Mass
Ma	–	Mach Number
P	W	Power
R	km	Range
Re	–	Reynolds Number
S	m^2	Surface Area
t	–	Time
V	m^3	Volume
V	N	Shear Force
V	V	Voltage
$\dot{V}$	m^3/s	Volumetric Flow Rate

List of Indices

APP	Approach
bat	Battery
cab	Cabin
cont	Contingency
div	Diversion
f	Friction
fus	Fuselage
HLD	Holding/Loitering
i	Induced
IC	Initial Climb to 1,000 m
inc	Incidence
inst	Installed
int	Interference
LDG	Landing
LE	Leading edge
m	Median
MAC	Mean Aerodynamic Chord
max	Maximum
min	Minimum
misc	Miscellaneous
P	Payload
prop	Propeller
req	Required
specific	Per Mass Unit
sys	System
TO	Take-off
tot	Total
tu	Turbulent
W	Wing

List of Abbreviations

ALT	Alternate.
AOA	Angle of attack.
BW	Box wing.
CB	Circuit breaker.
CFD	Computational fluid dynamics.
CFRP	Carbon fibre reinforced plastic.
CHARGE	**C**arbon-neutral, **H**igh-efficiency **A**ircraft for **R**e**G**ional **E**lectric flight.
COG	Centre of gravity.
Dash 8	De Havilland Canada Dash 8 Q400.
DEM	Delivery Empty Mass.
DEP	Distributed electric propulsion.
DIN	Deutsches Institut für Normung.
DOC	Direct operating costs.
DoD	Depth of discharge.
DP	Design Point.

EASA	European Union Aviation Safety Agency.
EC	Energy consumption.
ECS	Environmental control system.
EIS	Entry into service.
EN	Europa Norm.
FRP	Fibre reinforced plastic.
HLD	Holding.
IAS	Indicated airspeed.
ICAO	International civil aviation organisation.
LFL	Landing field length.
MLM	Maximum Landing Mass.
MMEI	Micro-multilayer multifunctional electrical insulation.
MTOM	Maximum take-off mass.
NASA	National Aeronautics and Space Administration.
OEM	Operating Empty Mass.
PAX	Passenger.
RAT	Ram air turbine.
ROC	Rate of climb.
SAF	Sustainable aviation fuels.
SE	Specific Energy.
SEP	Specific excess power.
SET	Specific excess thrust.
SKC	Seat kilometer costs.
SOC	State of charge.
SP	Specific power.
TLAR	Top level aircraft requirements.
TMS	Thermal management system.
TOFL	Take-Off Field Length.
TRL	Technology Readiness Level.
TW	Tube and wing.
VSV	Variable system voltage.
WIPS	Wing-ice protection system.
ZBM	Zero Battery Mass.

List of Figures

List of Tables

Rendering of CHARGE

1 Introduction

The world's temperatures are rising and water levels are climbing, all due to global warming and a massive increase in the amount of greenhouse gases in the Earth's atmosphere. The aviation sector alone was responsible for the emission of approximately one billion tons of CO_2 into the atmosphere in 2019. This represents about 2.5% of the yearly global emissions. The amount has almost doubled since 1990, as shown in figure 1-1. Regional short-haul flights, in particular, account for a large percentage of emissions [2].

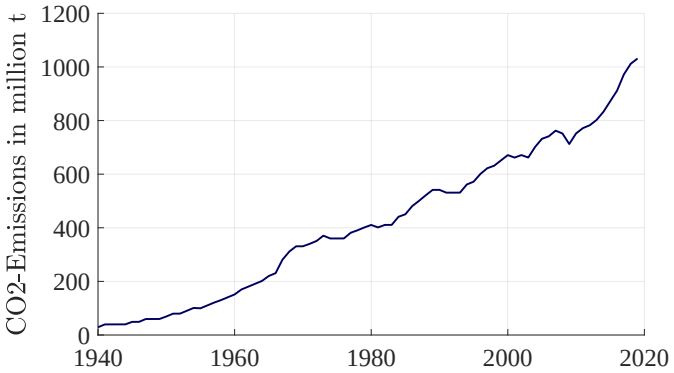

Figure 1-1: Global CO_2 Emissions Caused by Aviation 1940-2019 [2]

As a consequence of the above, the focus of this year's DLR Design Challenge is the development of sustainable solutions for short-haul flights. The challenge entails the creation of an aircraft concept that facilitates climate-friendly short-haul transportation on a specified airport network with a predetermined travel demand. With an entry into service (EIS) in 2050, the possibilities for using new innovative technologies are broad. The parameters for optimisation will be energy consumption (EC) per seat kilometer and seat kilometer costs (SKC). The proposed solution is **C**arbon-neutral, **H**igh-efficiency **A**ircraft for **R**e**G**ional **E**lectric flight (CHARGE). The following paper will provide an explanation of the aircraft's concept, as well as an analysis of the selected design range in terms of sustainability and economics.

2 Literature Review

Vries et al. [3] provides a good and detailed source of information for specific values and a comparison of different energy sources for aircraft with projections for 2030 and 2050. The authors have proposed a battery electric aircraft for 90-passenger (PAX) with a range of 800 km. While this concept employs a Li-Ion battery, which differs from CHARGE, the comparisons with SAF and hydrogen are valid and serve as a useful point of reference for evaluating battery electric concepts in comparison to other energy sources.

For more modern box wing (BW) configurations, the various works of Abu Salem and Palaia and their co-authors provide a useful framework for comparing BW configurations to conventional tube and wing (TW) configurations. In general, the Department of Civil and Industrial Engineering at the University of Pisa conducts extensive research

on BW aircraft. In "Comparative Analysis of Hybrid-Electric Regional Aircraft with Tube-and-Wing and Box-Wing Airframes" the authors present a comprehensive, multidisciplinary comparison of BW and TW aircraft concepts for the same flight mission. This provides insights into the comparative weight and energy savings associated with a BW configuration. Building on their previous research the authors Abu Salem, Palaia, and Quarta [5] introduce a detailed comparative analysis of the operating costs and environmental impact of a BW-aircraft in comparison to a TW-concept for the same design mission.

A principal source of reference for calculating the aerodynamics of the BW configuration is the comprehensive master thesis by Schiktanz [6] explaining the complete design process for a BW aircraft. This work also relies on earlier research from Finck, R. D [7], which presents a catalogue of mathematical formulas and diagrams to calculate the aerodynamic properties of a BW, including the interference of the upper and lower wings. For a more exact calculation of the aerodynamic properties such as wing lift distribution and drag, Diederich [8] is a valuable resource.

The works of Raymer [9], Torenbeek [10], Nicolai and Carichner [11] are valuable resources to estimate the mass of aircraft systems. The detailed work "Synthesis of Subsonic Airplane Design" by Torenbeek is a valuable source for mass estimations of aircraft main and subsystems. The estimations of Torenbeek are based on aircraft from before 1980. Since then, much progress has been made to reduce the weight of whole structures and systems. For some components, it is preferable to use estimations based on the work of Raymer. Another supporting input comes from "Fundamentals of aircraft and airship design" written by Nicolai and Carichner, which considers technological developments and provides estimates that account for advances in materials, such as the use of fibre reinforced plastic (FRP) and the integration of more electric aircraft systems.

The dissertation of Palaia [12] is a comprehensive source covering all aspects of the conceptual design of hybrid-electric BW aircraft. It is mainly used to establish all power requirements for CHARGE. Hepperle [13] proposes methods to specify the key parameters of a distributed electric propulsion (DEP) system in the preliminary design phase.

Girishkumar et al. [14] provides an overview of the potential of lithium air batteries and their projected use in the future. Several performance projections with regard to aviation, are provided by Sahoo, Zhao, and Kyprianidis [15]. Additionally Rahman, Wang, and Wen [16] provide further values and their future viability in "A review of high energy density lithium–air battery technology".

3 Market-Concept Analysis

As the aerospace industry and air traffic have struggled during the previous years, the Airbus Global Market Forecast for 2023 shows that air traffic in Europe has recovered fully, compared to 2019 [17]. Traffic flow between central and western Europe is expected to triple already in 2042. Along with jobs, financial opportunities and future technologies, the impact on the climate must not be forgotten. The Umweltbundesamt anticipates a rise in CO_2 emissions of at least 100 % [18], even though the fuel consumption per revenue passenger kilometer is already decreasing 2.9 % per year. This illustrates the necessity for the development of novel and innovative aircraft concepts like CHARGE. The following chapter will present a detailed analysis of the market and the conclusions that have led to the design concept.

3.1 The Search for a New Concept

The European Union has passed the legislation act RefuelEU Aviation to promote the usage of sustainable aviation fuels and make flying in Europe less carbon-intensive. The objective of these new regulations is twofold: first, to reduce the carbon footprint of existing aircraft fleets that utilise kerosene equivalents and second, to pave the way for the utilisation of hydrogen as an energy carrier in the aviation industry. For now, the legislation has set goals until 2050, of which one is to increase the proportion of sustainable aviation fuels (SAF) to at least 70 % in European airports [19, 20].

Although these goals are ambitious, they nonetheless extend the timeline for achieving true carbon-neutral aviation beyond 2050. In this timeline, only two energy sources will be available: hydrogen and SAF. In contrast, electricity as an energy carrier has a different outlook due to the availability of low-carbon, renewable electricity generation. Thus far, no European legislation has been enacted with the explicit objective of achieving 100 % renewable electricity generation by 2050, only a wider goal to achieve climate neutrality by 2050. According to projections, the share of renewable electricity production in 2050 should reach 84 % to 94 % [21, 22]. It can be reasonably assumed that electricity as an energy carrier will be less carbon-intensive than aviation hydrogen or SAF.

A more detailed analysis of the grid-to-shaft energy efficiency of SAF, hydrogen and electricity reveals that electricity as an energy source provides an unbeatable advantage, as demonstrated in table 3-1. It is evident that considerable losses are incurred at each stage of the production process and transportation of hydrogen and SAF until it is loaded onto the aircraft (grid-to-tank). The main losses occur during the highly energy-intensive processes of electrolysis and direct air capture. Even after the energy carriers have been loaded onto the aircraft, there are still high losses to convert the stored energy to propulsion (tank-to-shaft). To output 1 kWh of energy to propel the aircraft using a battery electric powertrain, only an extra 30 % of energy has to be produced in the grid, compared to over 300 % for hydrogen and 900 % SAF. This comparison also extends to the equivalent CO_2 emissions per PAX-km, where battery electric aircraft are estimated to emit approxemately 5 $g/_{PAX \cdot km}$, while hydrogen and SAF are found to emit between 50 to 120 $g/_{PAX \cdot km}$ [1][3]. Coincidentally, battery electric aircraft and electric vehicles have a very similar environmental impact. It is therefore evident that a battery electric powertrain will offer a significant advantage in terms of both cost and environmental impact. In other words, "if the missions can be flown electrically, then it should be flown electrically" [3].

Table 3-1: Energy Pathways for Different Propulsion Systems, Vries et al. [3]

Power-to-liquid synthetic fuel (eSAF)																	
Green electricity		Grid transport[a]		H_2 electrolysis		CO_2 direct air capture[b]		e-Fuel synthesis		Transport		Gas turbine				Propulsion	
5 ∼ 9 kWh	>	94 - 100%	>	70 - 71%	>	63 - 68% or 100%	>	65 - 73%	>	98 - 99%	>	38 - 42%			>	**1 kWh**	
Hydrogen turbine																	
Green electricity		Grid transport[c]		H_2 electrolysis		Lique-faction				Transport & boil-off[c]		Gas turbine				Propulsion	
4 ∼ 5 kWh	>	94 - 97%	>	70 - 71%	>	70 - 83%	>			97 - 98%	>	38 - 42%			>	**1 kWh**	
Hydrogen fuel cell																	
Green electricity		Grid transport[c]		H_2 electrolysis		Lique-faction				Transport & boil-off[c]		Fuel cell		Electric motor[d]		Propulsion	
3 ∼ 4 kWh	>	94 - 97%	>	70 - 71%	>	70 - 83%	>			97 - 98%	>	50 - 60%	>	85 - 95%	>	**1 kWh**	
Battery electric																	
Green electricity		Grid transport						Battery charging		Battery discharging				Electric motor[d]		Propulsion	
∼ 1.3 kWh	>	94 - 97%	>				>	95 -96%	>	95 - 96%	>			85 -95%	>	**1 kWh**	
										⟵ **Grid-to-tank**		⟶ **Tank-to-shaft**					

[a] 100% if renewable electricity is produced at fuel production site
[b] 100% if carbon is available from elsewhere (e.g., non-clean steel or cement production)
[c] Assuming hydrogen is produced at airport
[d] Includes losses of cables, inverters, etc.

The energy source is not the only configuration aspect that should be taken into account when designing a new clean sheet aircraft. Both the type of powertrain and the wing configuration also greatly influence the performance and efficiency of the concept. In table 3-2 an overview of the comparison of different aircraft configuration concepts for the given route network is provided. The different concepts are qualitatively rated based on research of the given literature and the feasibility study described in the section 3.2. The scores are based on projections until EIS in 2050 to find the most promising concept from each category for the defined route network.

A battery electric concept is the most viable solution due to the very high projected availability and low emissions, as described above. The availability scores takes into account projected total production and required use in other sectors. Here hydrogen concepts have a lower availability score as the produced hydrogen is sorely needed in industrial sector. The forecast prices for the individual energy sources are defined in the assignment, but the total cost listed in the table is based on the results of the total fuels cost estimated in the feasibility study described in 3.2. Only the feasibility of the battery electric concepts is rated lower than the alternatives due to the amount of research necessary into Li-air batteries and how to safely incorporate them in aircraft. As the design of a new type of high voltage electrical systems is still in a state of needed research, the feasibility is ranked lower.

For possible propulsion concepts, distributed propulsion combined with a conventional propeller motor score the best. Ducted fans, whether electric or turbine-powered, also show promise, however, they possess lower efficiency and higher mass. The feasibility for distributed electric propulsion is rated highly, as this topic is currently of high research

[1] According to Vries et al. [3], in this CO_2-equivalent the following emissions are accounted for: emissions produced during the mission, emissions generated in the production of the energy consumed during the mission, and emissions produced in the manufacturing of batteries. Emissions generated in the manufacturing process of the vehicle or the infrastructure are not included in this analysis. For in-flight emissions, both CO_2 and non-CO_2 effects are considered, which can be significant.

interest and smaller prototype aircraft are already being developed like the X-57 Maxwell by NASA or the Lilium Jet [23, 24].

For the wing configuration the two most promising options: a strut braced high aspect ratio wing and a BW are considered. Both are considered to have a good to very high efficiency and feasibility score. The strut braced wing has a lower score in the operations due to the high wingspan that might limit operation of the aircraft at some smaller regional airports or make the operations in the airport more difficult or time consuming. A BW design can achieve a lower structural mass compared to a strut braced wing, but incurs a penalty for higher complexity for integrating the wing into the aircraft structure.

Table 3-2: Comparison of Different Concepts for Energy Source, Propulsion and Wing Configuration

Concepts for Energy Source						
Concept	**Parameter**					
Energy Source	**Availability**	**System Mass**	**Efficiency**	**Feasibility for EIS**	**Cost (Price)**	**Total Score**
Battery Electric	+ +	-	+ +	+	+ + (0.038 \$/kWh$_{2019}$)	**7**
Hydrogen	0	+	0	+ +	0 (0.097 \$/kWh$_{2019}$)	**3**
Hydrogen Electric Hybrid	0	0	+	+ +	+	**4**
SAF Electric Hybrid	+	+	- -	+ +	- - (0.104 \$/kWh$_{2019}$)	**2**
Concepts for Propulsion						
Propulsion Configuration	**System Complexity**	**Efficiency**	**Redundancy**	**Feasibility for EIS**	**System Mass**	**Total Score**
Distributed Propulsion	-	+ +	+ +	+	+	**5**
Ducted Fan	+	+	0	+ +	0	**4**
Propeller	+	+	0	+ +	+	**5**
Concepts for Wing Configuration						
Wing Configuration	**Structural Integration**	**Efficiency**	**System Mass**	**Feasibility for EIS**	**Operations**	**Total Score**
Strut Braced High Aspect Ratio Wing	+	+	0	+ +	-	**3**
Box Wing	**0**	+ +	+	+	+	**5**

To determine the final configuration, synergies between the single concepts are analysed that can further increase the final efficiency of the aircraft. The energy sources do not have much of a synergy effect with the wing configuration. A SAF electric hybrid would integrate better with a strut braced wing, as the fuel can be more easily stored inside a single wing. A much more important effect is seen in the interplay between energy source and propulsion configuration. Here it is identified that a distributed propulsion concept would integrate well with a battery electric or highly hybridised energy source to allow the use of multiple smaller electric motors spread along the wing. Using this effect it is possible to achieve considerable increases in the efficiency of the aircraft for both wing configurations. Thus, the most promising concept should utilise a battery electric distributed propulsion powertrain combined with a BW. Table 3-2 also presents the scores for each component, together with a breakdown of these scores.

3.2 Analysis of the given Network

Prior to the detailed design process, a feasibility study was performed to assess the most critical parameters. This includes maximum take-off mass (MTOM), specific Energy (SE) and EC for both a battery electric and hydrogen powered concept based on the required range of $R = 1{,}144\,\mathrm{km}$ [2]. This was achieved using the Breguet range equation and methods for energy consumption estimations [25, 26]. The results of the feasibility study for the SE of the battery are presented in figure 3-1. The diagram shows a surface plot that takes into account empty mass fraction and the SE of the battery to visualise the change in MTOM based on the two parameters. The diagram shows that the usable SE of the battery should be greater than $500\,^{\mathrm{kWh}}/_{\mathrm{kg}}$ to prevent a rapid increase in MTOM with minor alterations to the concept. Furthermore, the total energy required to fly the distance is estimated for both the battery electric and hydrogen electric concept in figure 3-2.

Figure 3-2 demonstrates that an electric powered aircraft with a SE of $1{,}200\,^{\mathrm{Wh}}/_{\mathrm{kg}}$ will require less energy to complete a given trip than a hydrogen powered aircraft.

[2] longest distance of the indirect route network HAM-EDI with an added diversion range $R_{div} = 250\,\mathrm{km}$

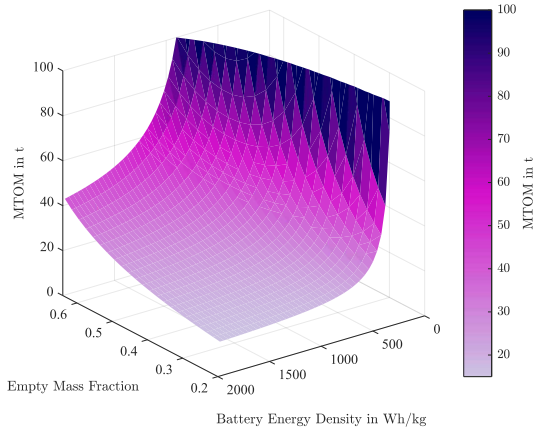

Figure 3-1: MTOM over Battery SE and Empty Mass Fraction for a Range of 1,144 km

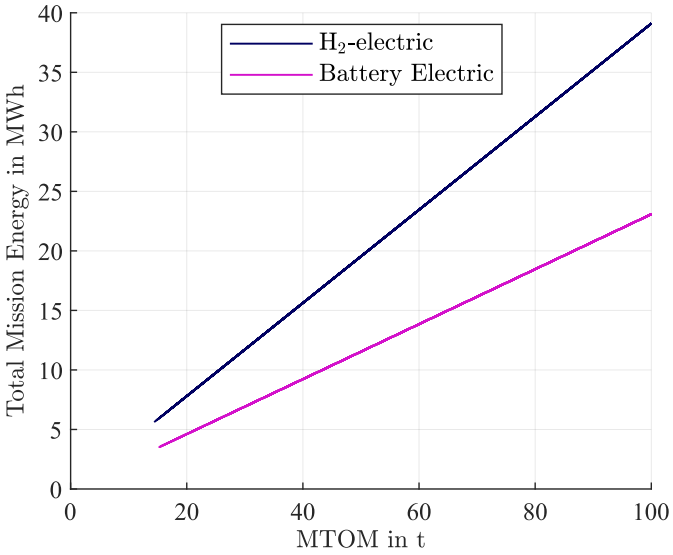

Figure 3-2: Comparison of Total Energy for a Battery Electric and Hydrogen Concept for a Range of 1,144 km

The given air traffic network consists of 16 flight connections, including European cities such as Hamburg, Edinburgh, Sarajevo and Trondheim. The flight range varies between 361 and 1,480km and can be reduced to 894 km by implementing stopovers. A passenger demand per week is given and must be fulfilled. The indirect flight network is shown in table 6-1. Further size limiting specifications are the used airport slots in Hamburg, a minimum of 42 slots must be used, a maximum of 276 may not be exceeded. Thus, a design for 60-120 PAX with 4-, 5- and 6-abreast configurations are possible. For each abreast and PAX configuration, it is possible to observe and evaluate the network realisation depending on factors such as cruise speed, turnaround time and a resulting number of planes. The feasibility of size and capacity must be considered carefully. A design for 120 PAX and a 4-abreast configuration has a relatively long fuselage that complicates the BW location, however the desired aerodynamic distance between the two wings does not fit on a short fuselage for 60 PAX - 6 abreast. The complex iteration described in chapter 7 is used to produce flying configurations as shown in figure 3-3 where the location of the centre of gravity (COG), the area load and the operational decisions of a design are valid.

The designs can be evaluated by introducing a scoring system in which each EC and SKC are ranked from best to worst and are combined to produce a total score calculated using the equation eq 3-1. A factor between the two scores can implement the trade-off, whether the design focus is on an environmental or financial optimisation. The primary focus of CHARGE is to reduce EC and thus reduce the total mass and resource usage of the battery. Since operational aspects outweigh airlines' purchase decisions, the impact on direct operating costs (DOC) is not neglected. Thus, the design is optimised with a weighting of 70 % on EC and 30 % on DOC. Figure 3-3 shows, most of the designs for the indirect connections have better scoring. Limiting the design range results in a lower battery mass and thus in a lower MTOM, which yields a higher efficiency. Also, larger PAX capacities result into less planes needed for network realisation with lower DOC and less total flights and thus a better financial and environmental performance.

$$\text{Score} = \frac{\text{EC}_{\text{max}} - \text{EC}}{\text{EC}_{\text{max}} - \text{EC}_{\text{min}}} \cdot \text{F}_{\text{energy}} + \frac{\text{SKC}_{\text{max}} - \text{SKC}}{\text{SKC}_{\text{max}} - \text{SKC}_{\text{min}}} \cdot \text{F}_{\text{cost}} \qquad \text{(eq 3-1)}$$

The best configuration seems to be the 5-abreast - 110 PAX design for the given design range regarding the indirect flight connections.

4 Concept Characterstics

The field of commercial aircraft design has found a configuration in tube and wing designs with two to four engines that is highly versatile, reasonably simple to manufacture and also open for later modifications and advancements. Furthermore, airport infrastructure over the last 70 years has been tailored to such designs. The new concept of aircraft

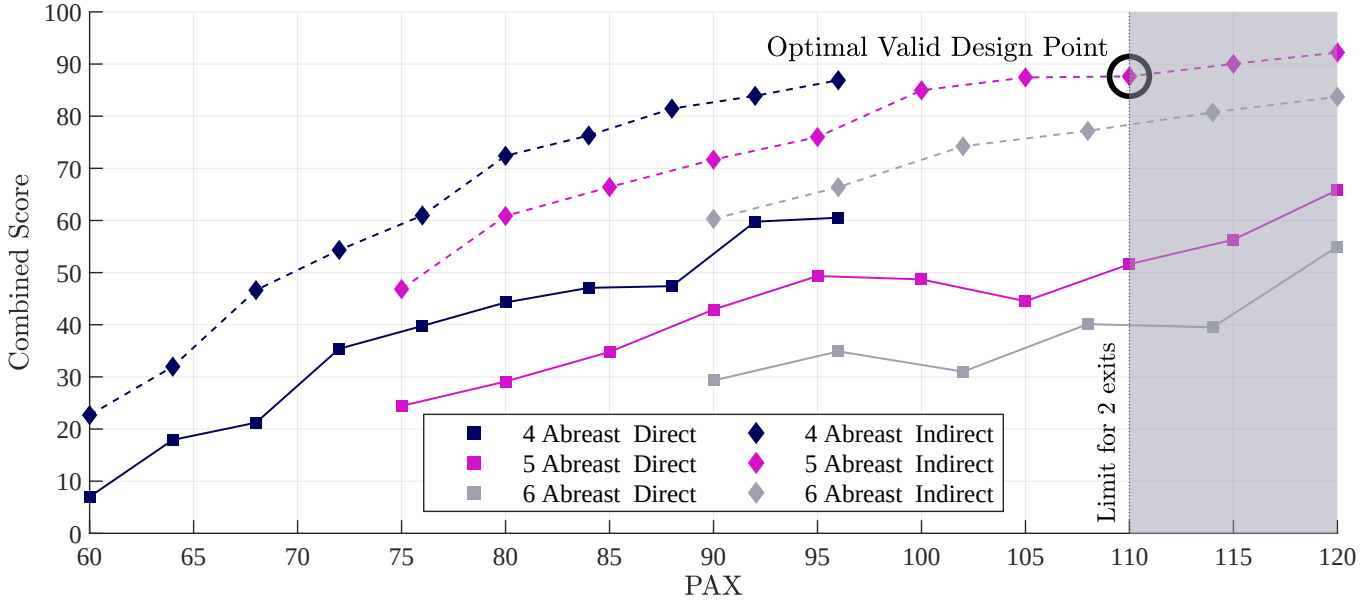

Figure 3-3: Scoring of Different Cabin Configurations and PAX Values for $Ma_{CR} = 0.57$, Weighting 70:30 % for EC:SKC

should therefore use the experience and knowledge gained in the last decades of aerospace engineering to define a new type of aircraft that is environmentally friendly, efficient, and economically viable. CHARGE arguably offers all the benefits of conventional TW designs while combining new and upcoming advances in propulsion technologies and structural design.

CHARGE builds upon the established TW concept by integrating a more efficient BW with a sophisticated and efficient battery-powered distributed electric propulsion system. The advantages of the TW concept are maintained by having a versatile and modifiable structure that can easily operate in all airports. As CHARGE is a battery electric aircraft, its CO_2 emissions and operating costs are unbeatable by hydrogen- or SAF-powered alternatives. The following chapters will present the concept in further detail and list the main parameters.

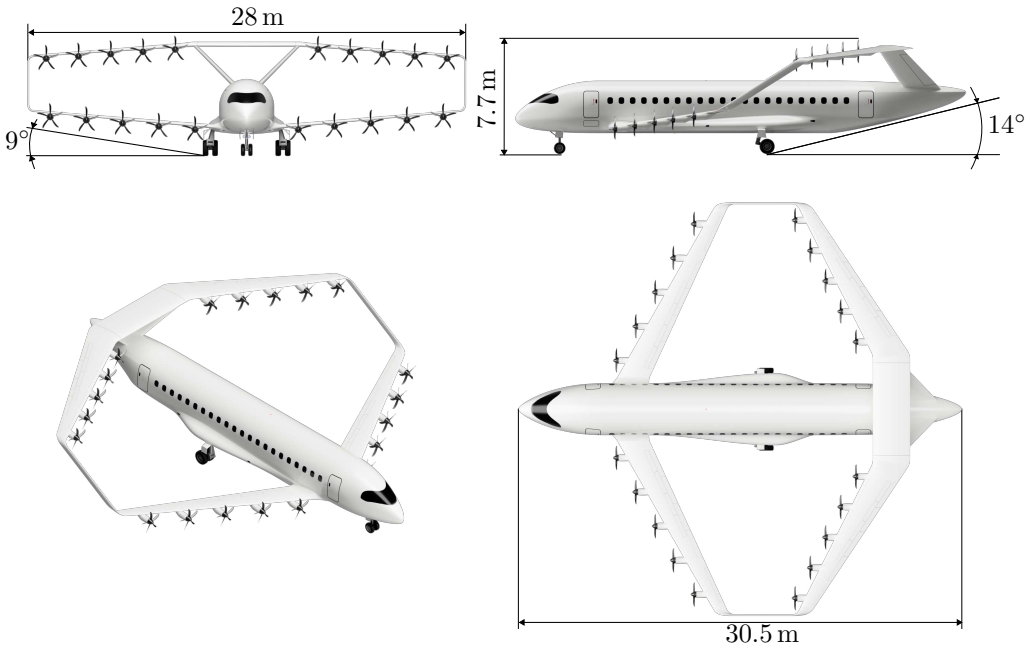

Figure 4-1: Three Sided View of Aircraft

The box wing, also known as a Prandtl wing was proposed in 1924 by Ludwig Prandtl as a configuration with low induced drag and thus high efficiency [27]. A BW resembles a biplane from the front, but from the side it is noticeable that the lower and upper wings are offset in the longitudinal direction and connected at the tips by winglets. The winglets act as barriers to reduce the strength of the vortexes formed at the tip of the wings. As an effect, the induced drag is considerably reduced. The wings can achieve a more uniform lift distribution along the wingspan and thus a higher wing load as visible in figure 5-9. To further increase efficiency, the upper wing is positioned above the V-tail to increase the vertical distance between the wings.

Another effect of the connected wings is their structural stability as the forces and moments created by the aerodynamic forces do not have to be carried by a single wing root, but are transferred over the vertical elements and shared by both wings. The forces and moments on the upper wing are carried into the fuselage structure over the V-tail. This also reduces the total weight of the wings, although the aerodynamic loads near the tips of the wings are higher compared to a conventional wing. As a positive effect the Operating Empty Mass (OEM) of a BW aircraft can be lower then a conventional TW configuration with the weight savings coming from the lower combined weight for the fuselage and wing group [4].

CHARGE is equipped with a DEP System on both the upper an lower wing. As a result, this concept benefits from higher propulsion efficiency, lower noise emissions and improved low-speed characteristics. CHARGE is a full-electric aircraft. Meaning there is no need for a hydraulic or pneumatic system. All systems are powered by the four lithium-air battery packs incorporated into the fuselages underfloor section. To control the aircraft, a combination of the rudders in the V-tail, the control surfaces on both wings, the horizontal morphing wing rudder and differential thrust of the DEP system is to be used.

Combining the high aerodynamic efficiency and lower structural mass of a BW leads to a configuration that can achieve the necessary lift and efficiency with a lower wingspan than conventional configurations. This gives CHARGE an important advantage when operating in the proposed route network with mostly smaller regional airports as the wingspan of the aircraft b of 28 m is classified as ICAO Class C ($24\,\text{m} < b < 36\,\text{m}$) [28] and suitable for all the proposed airports. The 28 m wingspan allows CHARGE to move and use all facilities at airports without obstacles. The C classification will also reduce fees as the aircraft can use smaller parking stands.
The three sided view of CHARGE is shown in figure 4-1. All key specifications are summarised in table 4-1.

Table 4-1: Key Specifications of the Aircraft, Powertrain and Wing

Aircraft	
Parameter	**Value**
MTOM	39,095 kg
m_p	10,450 kg
Ma_CR	0.57
H_CR	7,500 m
PAX	110
Seating	5 abreast
b	28 m
l_AC	30.5 m
ICAO code	3C
A_w	98.4 m^2
$C_\text{L,CR}$	0.45
$C_\text{D,CR}$	0.16
R	894 km
(G/F)	3,896 N/m^2

Powertrain	
Parameter	**Value**
SE_bat	1,200 Wh/kg
m_bat	8,924 kg
V_bat	12.17 m^3
E_tot	12.17 MWh
P_inst	6.24 MW
N_motor	20
η_system	93 %

Aircraft Performance	
Parameter	**Value**
TOFL	1,410 m
LFL	1,303 m
$c_\text{IC,max}$	6.7°

Wing		
Parameter	**Lower Wing**	**Upper Wing**
b	28 m	28 m
h_w	5.5 m	
A_w	Combined: 98.4 m^2	
	45.4 m^2	53.0 m^2
α_inc	2.3°	1.8°
C_L	Combined: 0.45	
	0.55	0.40
L	Total: 383,400 N	
	203,500 N	179,900 N
Δ_L	53 %	47 %
φ_LE	30°	−27°
λ	0.4	0.35
Γ [3]	5°	−4°

[3]The positive dihedral angle is for the lower wing and the negative anhedral angle for the upper wing

Table 5-1: Breakdown of Mass Estimation

Group Indication		Mass in t	% of MTOM
Airframe Structure	Wing Group	6.00	15
	Fuselage	3.72	10
	Tail	0.31	1
	Landing Gear	1.55	4
	Surface Control	0.58	2
	Group Total:	12.16	31
Propulsion Group	Motor, Propeller & -control, Inverter, etc.	1.29	3
Electrical Group	Actuators, Cables & misc.	1.66	4
Airframe Services & Equipment	Instruments, Furnishing & Equipment, etc.	3.26	8
Delivery Empty Mass (DEM)		18.37	47
Operational Items	Safety, Seating, Provisions, etc.	1.36	3
OEM		19.72	50
Payload		10.45	27
Zero Battery Mass (ZBM)		30.17	77
Battery Mass		8.92	23
MTOM		39.10	**100**
Max. Battery Mass Increase	(for Holding (HLD) & Alternate (ALT))	0.61	2
Maximum Landing Mass (MLM)		39.72	102

5 Technical Characteristics

The following sections provide a more detailed account of the construction of the aircraft and an examination of the principal systems and their underlying design assumptions. For each system, the chapters also provide a concise overview of the engineering methods and sources used to design and calculate the characteristics of the aircraft. An overview of the single masses on the aircraft and how they were calculated is given. Furthermore, the design and calculation of the wing aerodynamics, including the relevant mathematical formulas, is discussed. In the final chapters, the performance characteristics, including the energy usage and energy breakdown during a mission are discussed in greater detail.

5.1 Mass Estimation

The chosen PAX capacity and design range but also the aircraft configuration are key aspects which influence the mass estimation. Most of the detailed evaluation can be performed, using statistical methods of Torenbeek [10], Raymer [9], Nicolai and Carichner [11]. Given the unconventional nature of the CHARGE concept, particularly with a BW and electric propulsion, it is necessary to make assumptions regarding a possible mass adjustment. As a structural wing concept would be too complex to design, the wing is considered as two separate wings, each lifting part of the total aircraft mass. Additionally, two connecting winglets for structural support are taken in account of. For the structural benefits of a BW configuration, realised by use of modern composite structures, a conservative reduction of 20 % is made. For the fuselage, landing gear and surface control group, Raymer suggests technology factors for structural mass reduction of 10 %, 5 % and 40 %. A detailed mass estimation is shown in table 5-1. The MTOM of CHARGE is relatively high, as the mass of the battery is much greater than the mass of the fuel for comparable short-haul aircraft. CHARGE is 8.6 t heavier than the comparable reference aircraft De Havilland Canada Dash 8 Q400 (Dash 8), although it carries only 1.9 t more payload.

5.2 Aircraft Systems

This section presents the individual aircraft systems, their concept design and integration. As CHARGE is a full electric aircraft, the propulsion system depends on electric motors, power electronics and of course a battery system. Furthermore this concept does not rely on any hydraulic or pneumatic system but instead utilises electric actuators and an electric environmental control system (ECS). The placement of all different Aircraft Systems is illustrated in figure 5-1.

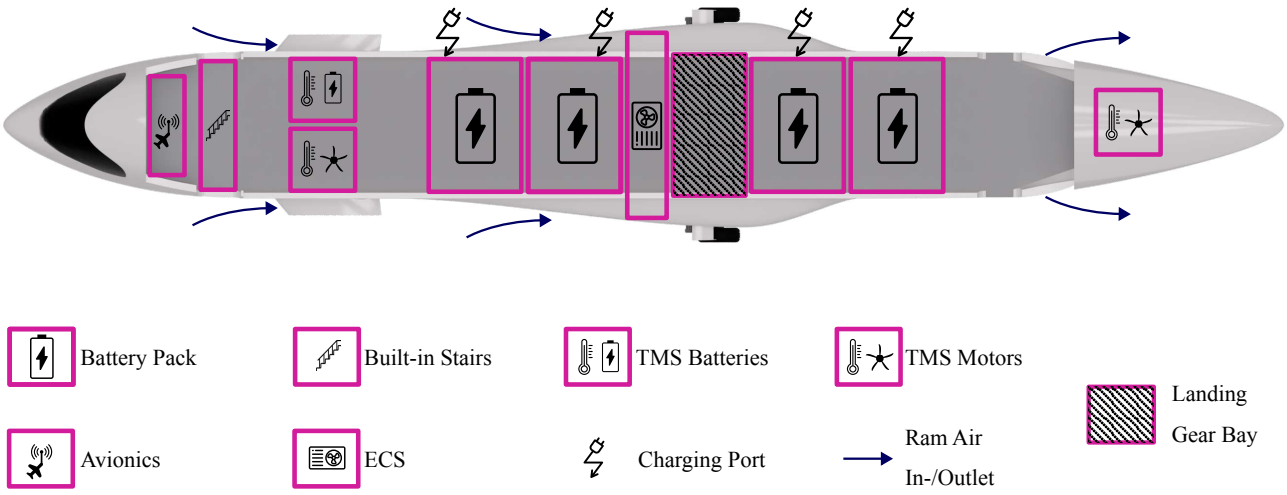

Figure 5-1: Display of most Relevant Aircraft Systems

5.2.1 Distributed Electric Propulsion System

DEP is a variant of a propulsion system in which the thrust is distributed across the span of the aircraft's wing by a number of electric propulsion units. A well-designed DEP system offers several advantages over traditional propulsion systems. One of the key benefits is an enhanced aerodynamic efficiency that mainly results from an increase in the total disc area A_{Prop} compared to similar traditional propulsion systems [29]. This causes the additional effect of reduced noise emissions [29]. In particular, during low-speed flight, the aircraft is able to maintain greater rudder authority due to the accelerated airflow around the wings. At the same time, this increases the effectiveness of the high-lift devices, resulting in a shorter, take-off and landing distances.

In order to make use of and quantify these potential advantages, a detailed analysis of the aeropropulsive interaction is mandatory [29, 13]. Such an analysis is not feasible for a concept design. Therefore Hepperle [13] proposes a method to asses the most important design parameters, such as the number of engines, propeller diameter and engine position. The general idea behind this method is to compare the total disc area A_{prop} of the DEP system to a reference aircraft, in this case the Dash 8. A similar total disc area leads to approximately the same propulsion efficiency η_{prop}, while choosing a larger total disc area improves the overall efficiency [13]. Assuming the motors are evenly distributed over the entire wingspan, increasing the number of motors N_{motor} results in a smaller total disc area. So using fewer motors should in theory result in a greater efficiency. At the same time lowering the number of motors increases the total system mass because of the larger propeller diameter d_{prop} [13].

Considering the total disc area A_{prop}, but also the system mass and complexity, an optimal number of propulsion units for CHARGE was determined to be twenty, of which ten are located on each wing. There are no propulsion units placed on the morphing trim area between both V-Tails, as the motor fairing would interfere with the morphing structure. For reasons of simplicity in design and production, all propulsion units use the same diameter for the propellers. This leads to slightly different tip to tip distances for lower and upper wing, due to different usable wingspans. The propeller diameter is chosen so that sufficient clearances are maintained between the propeller tips, fuselage and ground. The configuration above ensures a total disc area A_{prop} 1.8 times greater than the reference aircraft, while the total system mass is 34 % lighter [30, 31].

In addition to the number of motors, the positioning on the wing also has a decisive influence on the system efficiency [13]. It is desirable to position the propellers in a location where the local flow velocity is as low as possible [13], which is usually below the wing. The engines of CHARGE are positioned under the wing in such a way that this effect is utilised as far as possible without the drag of potentially extended engine nacelles leading to greater efficiency losses than are gained by the placement.

To account for the positive effects of a DEP in the aircraft performance calculations, it is assumed that CHARGE

is able to perform its takeoff in 10% less distance compared to the standard configuration which is a conservative estimation[32]. Aside from the better take-off performance, there is a higher efficiency expected in cruise due to the high total disc area compared to the Dash 8. The engines of CHARGE are positioned under the wing in such a way that this effect is utilised as much as possible without the drag of potentially extended engine nacelles leading to greater efficiency losses than are gained by the placement.

5.2.2 Propulsion Unit

Each propulsion unit consists of a five-bladed propeller and the nacelle accommodating the Motor and Inverter as shown in figure 5-2. The specific power (SP) for the motors are assumed to reach 16 $^{kW}/_{kg}$ by 2050 using advanced super conducting high efficiency technology currently developed by National Aeronautics and Space Administration (NASA)with a proposed efficiency η_{motor} of 99 % [33]. To give each propulsion unit the ability to be controlled individually, and for reasons of high redundancy, each motor is equipped with its own inverter with a SP of 20 $^{kW}/_{kg}$ at 99.5 % efficiency $\eta_{inverter}$ [34]. This additionally enables the propulsion system to implement thrust vectoring abilities. The propeller system incorporates a pitch control system to ensure maximum propulsion efficiency in all phases of flight. The tip speed of the propellers is kept similar to that of the reference aircraft, resulting in a speed n_{prop} of 2,440 rpm. This propeller speed is adjusted to the engine speed with a small gearbox, which is installed between the engine and propeller. The engine speed n_{motor} is expected to be approximately 6,000 rpm, resulting in a gear ratio $i_{gearbox}$ of $^{1}/_{2.5}$.

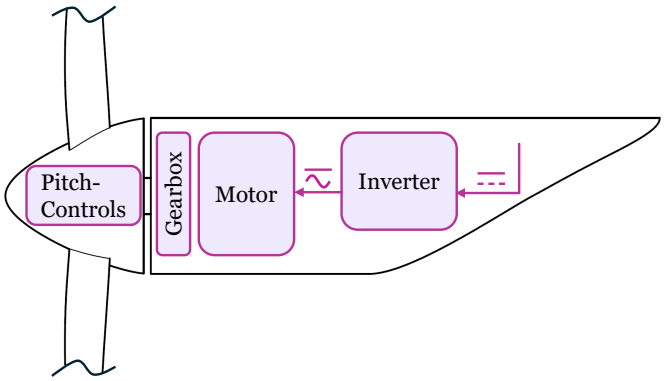

Figure 5-2: Schematic of the Propulsion Unit

Table 5-2: Propulsion Parameters

Parameter	Value	Source
SP Motor	16 $^{kW}/_{kg}$	[33]
η_{motor}	99 %	[33]
SP Inverter	20 $^{kW}/_{kg}$	[34]
$\eta_{inverter}$	99.5 %	[34]
d_{prop}	1.7 m	-
n_{prop}	2,440 rpm	-
n_{motor}	6,000 rpm	-
$i_{gearbox}$	$^{1}/_{2.5}$	-
A_{prop}	46.3 m^2	-

5.2.3 Power Distribution

With the all-electric architecture of CHARGE, power distribution is a key aspect of the design process to ensure safe and efficient operation. The power distribution is based on a three-bus multi-feeder architecture as shown in figure 5-3. This layout provides an excellent redundancy while maintaining light weight [35].

All motors are directly connected to two independent buses, while each main bus (five to seven) is directly powered by two battery packs. This ensures that in the event of any single failure other than a direct motor failure, all motors can still be powered via an alternative route. The failure modes considered are direct battery pack failure, any random bus failure, and any cable failure. All cables, batteries and buses are sized for the corresponding worst case failure as described. In case of a severe electrical failure or the unlikely event of completely drained batteries, all inboard propulsion units are able to act as ram air turbine (RAT) and feed electricity back into the most critical systems such as the actuation system of the flight controls and avionics. Due to a higher potential system efficiency η_{sys}, the whole power distribution system is based on variable system voltage (VSV), which means that the decreasing battery voltage is not compensated for by converters, but rather is fed directly into the consuming systems [36]. The design system voltage is defined at 0 % state of charge (SOC). The high power demand of all-electric aircraft would lead to unbearably high currents with today's voltage level standards [37]. System voltages in the kilovolt range are necessary to enable efficient energy transport through the aircraft. Determining an optimal system voltage requires a detailed sensitivity analysis using the system masses and efficiencies [15]. For the preliminary design, 4 kV has been identified as a suitable system voltage V_{sys} on the basis of several studies [38, 36]. High voltage present

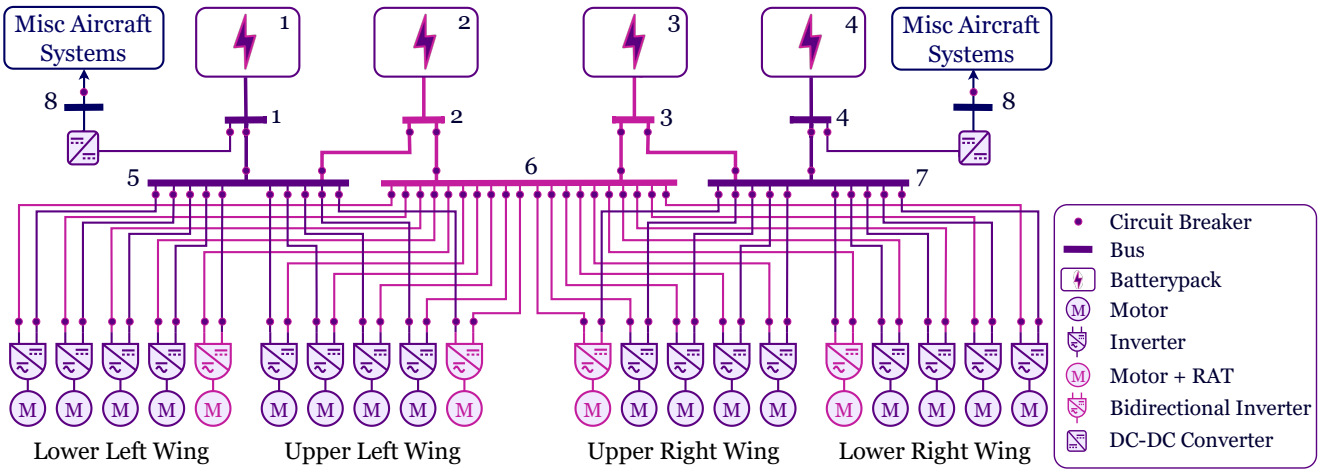

Figure 5-3: Schematic of the Power Distribution Architecture

a number of challenges. One of which is the higher risk of arcing at high voltage and altitude, which sets high requirements for cable insulation and routing [38]. There are currently no standards or regulations for high voltage systems in aircraft applications [37]. To address some of these challenges, CHARGE uses advanced micro-multilayer multifunctional electrical insulation (MMEI) [39]. Hereby multiple functions are incorporated into the insulation by combining different materials with different properties. These functions include corona partial discharge resistance, moisture barrier, electromagnetic interference shielding, thermal management and mechanical durability [39]. Another challenge when using high voltages is the safe and reliable disconnection of loads under load and in case of a fault. Therefore 95 circuit breaker (CB)'s are distributed along the power grid as shown in figure 5-3. The assumed SP of the CB's is 200 $^{\mathrm{kW}}/_{\mathrm{kg}}$ at 99.9 % efficiency [40] For all smaller non-propulsive loads a 1 kV bus is utilised and fed redundantly from packs one and four. These loads consist mainly of the actuation system, wing-ice protection system (WIPS), E-taxi system, lighting and galley loads. All avionics are powered from an additional 28 V bus and therefore meet today's standards. There is a total of 477 m high voltage cable routed through CHARGE. The cross-sections are estimated according to DIN EN 2853 [41] adjusted for aluminium as conductor. The individual cable and CB masses and positions are being considered in the mass estimation and determination of the COG.

5.2.4 Battery System

As seen in figure 3-1, the whole concept is dependent on sufficient SE of the batteries. Because of the high theoretical SE the batteries are chosen to be Li-Air. The cells consists of a lithium-anode and air-cathode separated by a solid electrolyte [14]. The chemical reaction appears as follows:

$$2\,\mathrm{Li} + \mathrm{O_2} \longrightarrow \mathrm{Li_2O_2} \quad \text{(Discharge)} \qquad \text{(eq 5-1)}$$

$$\mathrm{Li_2O_2} \longrightarrow 2\,\mathrm{Li} + \mathrm{O_2} \quad \text{(Charge)} \qquad \text{(eq 5-2)}$$

with the oxygen provided by the air [14]. Due to the chemical reaction, the battery mass m_{bat} and volume V_{bat} increases during discharge mid-flight. The lithium binds added oxygen as seen in eq 5-2. The operating mechanism of the battery shows an increase of 0.1 $^{\mathrm{g}}/_{\mathrm{Wh}}$. The volume increase is taken into account in the pack architecture as the needed volume is calculated for the discharged case. During discharge, additional oxygen is needed inside the cells, this is ensured by air flow provided by the four ram air inlets shown in figure 5-1. A total of approximately 11,700 m^3 of oxygen are required

Table 5-3: Battery Parameters

Parameter	Value	Source
SE	1,200 $^{\mathrm{Wh}}/_{\mathrm{kg}}$	[15]
Energy Density	1,000 $^{\mathrm{Wh}}/_{\mathrm{L}}$	[16]
SP	920 $^{\mathrm{W}}/_{\mathrm{kg}}$	-
Cycles Lifetime	1,500	[3]
Charging Power	3 MW	-

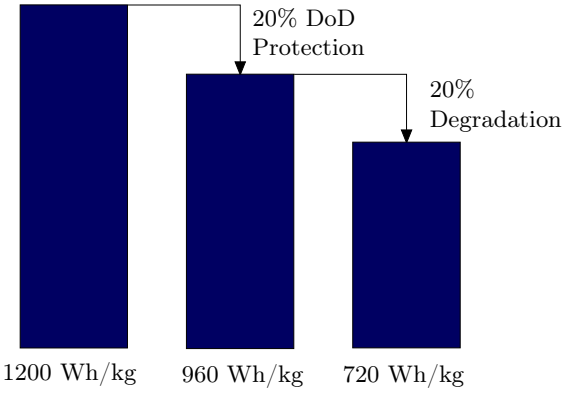

Figure 5-4: SE Breakdown

for the longest flight. Given that the batteries are supplied with ram air the inlets are sized for the most critical combination of required battery power and occurring dynamic pressure. This is the case at the start of the climb segment during acceleration to cruise speed. The required volumetric flow $\dot{V}_{\max}$ amounts to 1.35 $^{m^3}/_{s}$. During takeoff the batteries are supplied with compressed air from the ECS to account for the low ram pressure. A SE of 1,200 $^{Wh}/_{kg}$ [15] and energy density of 1,000 $^{Wh}/_{L}$ [16] are used. Due to 20 % depth of discharge (DoD) protection and 20 % degradation over lifetime, the effective SE is only 720 $^{Wh}/_{kg}$ [42], shown in figure 5-4. The batteries are split up into four packs, separated from each other, due to safety precautions. Each pack can be charged with one charging plug. Discharge and charge efficiencies (η_{charge}, $\eta_{\text{discharge}}$) are both 95 % [3]. A maximum SP of 917 $^{W}/_{kg}$ is required during discharge, which translates to approximately 0.7 C at 2.96 V cell voltage V_{cell} [43]. A charging power P_{charge} of 3,000 kW at 4 kV, which is also the system voltage V_{sys}, as described in section 5.3 is used, resulting in 1 C during the charging process. The lifetime of the cells is expected to be 1,500 full cycles [3]. At the end of their lifetime the packs are removed through access panels and replaced. Beside technical requirements the batteries need to ensure safety standards. In contrast to Li-Ion cells, thermal rundown due to overcharge is no concern with the Li-Air chemistry [14]. Although a fire is very unlikely an extinguishing system is installed. In case of fire, a powder is injected directly inside the pack to contain the flames. In addition, the pack is disconnected from the system and cooled until a safe landing and evacuation at the nearest airport is executed.

5.3 Thermal Management System and Environmental Control System

To achieve the highest possible energetic efficiency, CHARGE implements an integrated architecture of all thermal and environmental systems. Meaning that the ECS is able to utilise the excess heat from the thermal management system (TMS) and can allocate this heat to the WIPS and cabin if needed [44]. Furthermore the ECS works based on a design not relying on bleed air with an assumed power consumption of 68.4 kW during climb and descent and 42.8 kW in cruise flight [45]. The resulting energy usage is considered into the energy calculations in section 5.8.

The TMS consists of three independent cooling loops. This is due to different operating temperatures and positions in the aircraft [46]. The lower and upper wing each use a separate cooling loop which is supplied by ram air from the inlets located at the lower wing fairing and belly fairing. The third cooling loop is used to keep the battery at an optimal operating temperature. A SP of 3 $^{kW}/_{kg}$ for all cooling systems is assumed [47] . The actual TMS mass is therefore determined by the loss of each cooled system. The power consumption of the TMS itself is approximated with 1.5 $^{W}/_{kg}$ [47]. It is also possible to preheat the batteries in case of cold temperatures during ground time. The Energy is provided via the charging ports.

5.4 Structural Design

As visible in figure 4-1 the main gear is not located in the lower wing box, but is placed in the middle of the fuselage in a separate fairing, much like a typical high-wing aircraft. When the gear is retracted, it is stowed completely inside the fairing. The frame extends up to the lower wing box and houses much of the equipment for ECS. The aerodynamic shape of this fairing also allows it to act as a lift-

Figure 5-5: Structural Concept of Fuselage

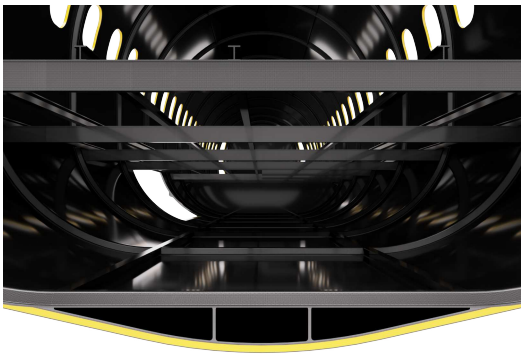

Figure 5-6: Sandwich Structure with Keel Beam

ing body, creating lift to compensate for the slightly increased drag. The structural design of the fuselage is shown in figure 5-5. The fuselage structure is a semi-monocoque carbon fibre reinforced plastic (CFRP) sandwich composite. The outer shell of the fuselage is composed of two layers of CFRP with a sandwich structure between them (colored yellow in the figure). This allows omitting the stringers in the fuselage structure without compromising the stiffness and strength of the structure. In the lower part of the fuselage, a keel beam made of CFRP is integrated directly into the sandwich hull structure. The fuselage is made of sections, each section being 1,524 mm long and spanning two windows. On the inside, frames running around the fuselage connect the transverse floor frames to the outer hull. Running longitudinally from the front to the rear of the structure, the floor beams are positioned under the seat tracks of the 3-2 abreast configuration. On the right side of the fuselage the openings for the doors, to access the batteries are visible. The structures pointing out of the fuselage on the right side are attachment points for the main gear and the V-tail. For a better overview the wing box for the lower wing is not shown. The calculated shear force on the wing box for the lower wing is $V_{\text{lower}} = 80\,\text{kN}$ and the root bending moment $M_{\text{lower}} = 429\,\text{kNm}$. The upper wing attached to the V-Tail experiences a shear force of $V_{\text{upper}} = 81\,\text{kN}$ and a root bending moment of $M_{\text{upper}} = 520\,\text{kNm}$.

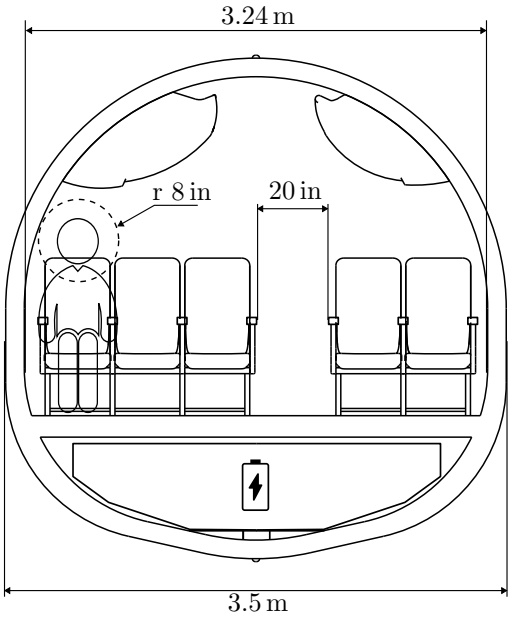

Figure 5-7: Cabin Cross Section

5.5 Cabin and Fuselage design

CHARGE is designed to accommodate 110 PAX in an all-economy layout. After careful iteration, a 5-abreast seating configuration was selected. A 4-abreast and 6-abreast configuration were also evaluated but ultimately deemed less optimal. A seat pitch of 30 in plus galleys, lavatories and emergency exits results in a cabin length l_{cab} of 22.12 m. To improve passenger comfort and operational flexibility, CHARGE is equipped with two lavatories. While a single lavatory would be sufficient for regional flights with 110 PAX, the additional lavatory ensures the operation of the aircraft even if one lavatory becomes inoperative. Two galleys capable of holding a total of five full-size-trolleys are installed in the front and back of the aircraft. The cabin layout is shown in figure 5-8. The 5-abreast seating configuration dictates a cabin width d_{cab} of 3.24 m, resulting in an overall fuselage diameter d_{fus} of 3.5 m. As shown in figure 5-7, the fuselage cross-section is adapted from a circular shape, with a widened lower half to accommodate the aircraft's batteries. Despite this adaptation, the fuselage retains the same diameter as a circle from top to bottom and left to right.

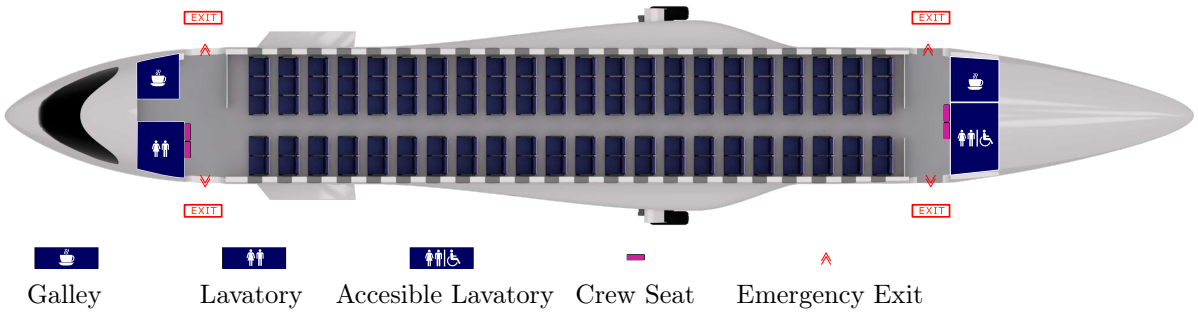

Figure 5-8: Cabin Layout

The fuselage is divided into three main sections. The cockpit section contains the cockpit, forward lavatory and galley as well as the L1 and R1 exits. The constant section contains the 22 rows of passenger seats. The tailcone-section contains the L2 and R2 exits along the aft galley and lavatory. Notably the taper from the side view begins two rows into the constant section, which allows for better tail clearance during rotation as illustrated in figure 4-1. All aspects of the cabin design comply with CS-25 regulations, such as maintaining an eight-inch head impact radius on hard monuments and minimum aisle width as shown in figure 5-7. CHARGE is equipped with two pairs of Type A sized emergency exits, enhancing the comfort of embarkation and disembarkation. For operational efficiency, these exits are certified as Type C, reducing the number of cabin crew required without compromising safety. Each pair of Type C exits is certified for 55 PAX, giving the aircraft a total maximum PAX capacity of 110, requiring three cabin crew.

5.6 Aerodynamics and Wing Design

The aerodynamic effects on the BW-configuration lead to its lower induced drag and thus higher efficiency compared to a more conventional high aspect ratio wing. To properly account for the efficiency increases in a BW-design specific calculations methods are used to design and optimise the wing. Here the dimensionless circulation distribution is used to calculate the lift and consequently the drag forces for the wing. Further estimations are used to calculate the drag of the various other components on the aircraft.

5.6.1 Aerodynamics

The geometry of the wing is visible in figure 4-1 and a detailed overview is listed in table 4-1. In the figure the horizontal and vertical stagger of the wing, the distance between the wing planes, $h_\mathrm{w} = 5.5\,\mathrm{m}$ and the positive and negative sweep angles φ_LE of the upper and lower wing are noticeable. Not clearly visible from the drawing is the taper ratio λ of both wings, with an equal outside wing depth for the lower and upper wing. This keeps the width of the connecting winglet constant over the winglets longitudinal distance and has structural advantages. As mentioned in chapter 4, the upper wing has an integrated morphing wing trim rudder in the aft rectangular section. Another less noticeable detail is the dihedral angle Γ of the lower wing and the anhedral angle of the upper wing. The combination of the dihedral-anhedral angles offer more ground clearance for the propellers on the lower wing and reduces the length and consequently weight of the the connecting winglets.

To calculate the aerodynamic characteristics of the BW it is necessary to divide the wing into a lower and upper surface and calculate the aerodynamic characteristics separately. It is thereafter possible to combine the aerodynamic characteristics of the lower and upper wings to calculate the combined characteristics of the BW, taking the interference of the two wings into account. The calculations are based on the work by Schiktanz [6] and Finck [7]. The increase of aerodynamic efficiency in a BW-design is due to the reduction of the vortex strength at the wing tips, because of the continuous vertical winglets. The reduced vortex strength decreases induced drag while increasing the lift distribution around the wing tip. The effect in efficiency is twofold by reducing drag and at the same time increasing lift. This effect is strongly influenced by the vertical stagger h_w of the single surfaces and the difference in the lift forces acting on the single surfaces [48]. For an exact calculation of the efficiency factor without comprehensive computational fluid dynamics (CFD)-simulations estimations according to Rizzo [49] were used in an iterative loop, taking into account the changes in geometry and aerodynamic forces.

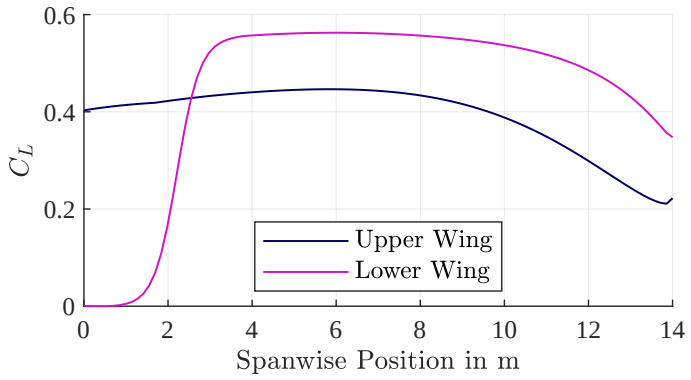

Figure 5-9: Lift Distribution Along the Lower and Upper Wing Along the Wing Span

$$\gamma(\eta) = \gamma_a(\eta) \cdot c_L + \gamma_b(\eta) \qquad \text{(eq 5-3)}$$

$$\gamma_a(\eta) = c_1 \frac{l(\eta)}{l_m} + c_2 \frac{4}{\pi} \sqrt{1-\eta^2} + c_3 \cdot f(\varphi, \eta) \qquad \text{(eq 5-4)}$$

$$\gamma_b(\eta) = k_1 \cdot c'_L \cdot \gamma_a(\eta) \cdot \left[\epsilon(\eta) - \int \epsilon(\eta) \cdot \gamma_a(\eta)\, d\eta \right] \qquad \text{(eq 5-5)}$$

$$K = \frac{e \cdot \Lambda}{\frac{c'_L}{2\pi} \cos \varphi_{25}} \qquad \text{(eq 5-6)}$$

The lift distribution of a BW is considerably different from a conventional single wing configuration. The distribution can be imagined in its most simple state as a sum of constant distribution over the whole span of the wing together with an elliptical distribution. As a result, the lift distribution at the wing tips does not approach 0, but remains at a relatively high value. In order to take into effect factors like the wing sweep and taper ratio, the lift forces along the wingspan were calculated using the method by Diederich for subsonic speeds [8]. In this method the wing geometry is taken into account to calculate the dimensionless circulation distribution γ for every local coordinate in the span wise direction η. This quantitative approach is valid for calculating the circulation on a wing for swept wings with a straight sweep angle at 25 % wing depth line φ_{25} and moderate aspect ratio up to the high subsonic range with satisfactory accuracy.

The first component of the circulation distribution γ_a in the equation eq 5-3 consists of the sum of an ellipse, depth and dihedral function and the second component γ_b in eq 5-3 describes the effect of wing twist. Both components for γ are dependent on coefficients C that can be calculated using a polynomial approximation. For brevity the coefficients are not further explained. It is important to note, these coefficients are dependent on the factor K (eq 5-6), describing the form factor of the wing. To take into account the increased efficiency of the BW, the original formula for eq 5-6 is multiplied with the Oswald factor e. It is of note, that the calculated value for $e = 1.4$ exceeds 1, an effect unique to the BW.

The result of the span wise lift distribution of one side can be seen in figure 5-9. The distribution of the lower wing starts with a value of 0 and reaches a nominal value by 2.5 m to consider the effect of the body, where the wing and its lift generation are interrupted. The high C_L value at the tips of the wings correspond to the expected effect of a BW and are comparable to the results in Schiktanz [6] and Palaia, Abu Salem, and Quarta [4].

Drag Estimations

To calculate the total drag, a multiprong approach was used. The distribution of the drag components is displayed in figure 5-10 The wing drag is calculated using the known lift distribution along the wingspan together with the local wing depth and is calculated for the upper and lower wing separately by using equation eq 5-7.

$$C_{\mathrm{D,W}} = \int C_{\mathrm{D,W,min}} + 0.03 \cdot C_{\mathrm{L}}^{6}(\eta) \cdot \frac{(\eta)}{l_{\mathrm{MAC}}} \qquad \text{(eq 5-7)}$$

To approximate the total wing drag it is necessary to divide the drag components into skin friction and pressure drag. It is noteworthy to note that, although it is customary to estimate a proportion of the airflow around the wing as laminar, this positive effect could not be relied upon for this concept due to the effect of the DEP on the wing inflow. Therefore, the minimum wing drag is calculated in accordance with the estimations proposed by Diedrich in equation eq 5-8, whereby the coefficient of friction $C_{\mathrm{f,tu}}$ is dependent on the Reynolds number Re, while the pressure drag coefficient k_{W} is dependent on the lenght-thickness ratio. A similar, simplified calculation is employed for the tailunit drag coefficient $C_{\mathrm{D,T}}$.

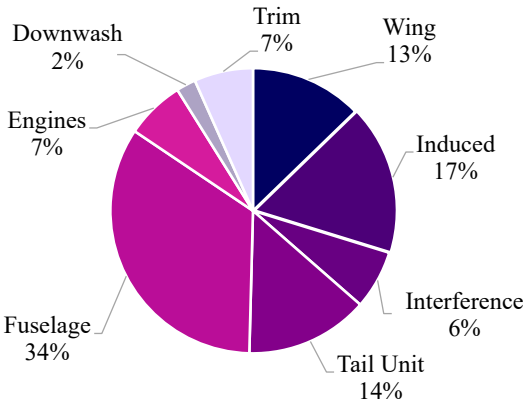

Figure 5-10: Detailed Drag Breakdown

$$C_{\mathrm{D,W,min}} = 2 \cdot C_{\mathrm{f}} \cdot (1 + k_{\mathrm{W}} \cdot \cos \varphi_{50}^{2}) \qquad \text{(eq 5-8)}$$

The transonic drag coefficient $C_{\mathrm{D,transsonic}}$ has been found to be nearly equal to zero and therefore not relevant. A significant drag component in our design is indicated by the downwash drag coefficient $C_{\mathrm{D,Downwash}}$, which is unusual compared to conventional aircraft designs. In conventional aircraft, the downwash drag coefficient $C_{D,Downwash}$, is negative due to the negative lift caused by the plane's tail unit. However, in our design, this drag component is positive because of the positive lift induced by the upper wing at the plane's back. The induced drag is calculated using the common formula depicted in equation eq 5-9. In this context, the Oswald factor e represents the positive influences of the BW on the induced Drag D_{i}.

$$C_{\mathrm{D,i}} = \frac{C_{\mathrm{L}}^{2}}{\pi \cdot e \cdot A_{\mathrm{W}}} \qquad \text{(eq 5-9)}$$

The final significant component-independent drag coefficient is the interference drag $C_{\mathrm{D,int}}$. This is approximated by applying equation eq 5-10, where n represents the number of analogous intersections between sub assemblies. Whereas

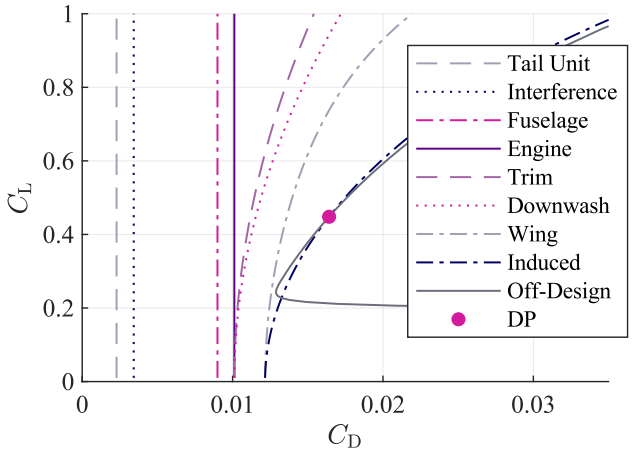

Figure 5-11: Cumulative Drag Polar

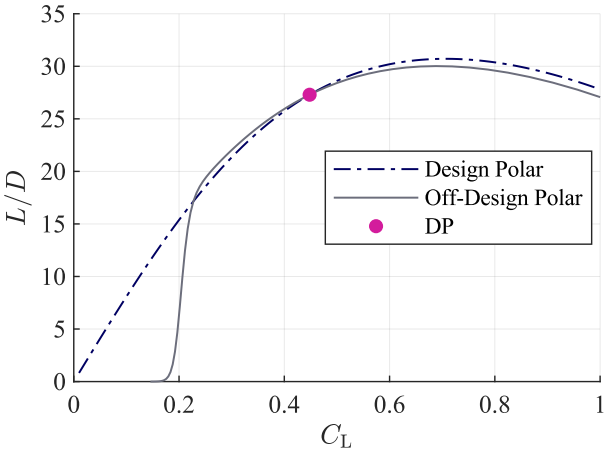

Figure 5-12: Lift to Drag Polar

l_{int} describes the interferences length.

$$C_{\text{D,int}} = \sum_{i=1}^{n} \frac{\frac{0.1369}{\text{Re}^{0.4}} \cdot l^2_{\text{intersection}} \cdot n}{A_{\text{w}}} \qquad \text{(eq 5-10)}$$

The drag for the other components also visible in figure 5-11 is calculated using approximations based on calculations carried out by Diedrich as well, wich are presented by Torenbeek [10]. They all depend on some variation of skin friction and pressure Drag. The final Design Point (DP) results in a lift coefficient of $C_{\text{L}} = 0.4480$ and a drag coefficient of $C_{\text{D}} = 0.0152$. This yields a lift to drag ratio of $^{L}/_{D} \approx 27$. This DP results in a stable configuration during cruise, as shown in figure 5-12.

5.6.2 High Lift Devices and Surface Controls

CHARGE is able to control its flight attitude through various control surfaces and its propulsion system. The placement of these surfaces can bee seen in the three sided view in figure 4-1. The roll movement is realised by the outboard ailerons on both wings trailing edges. The morphing trailing edge rudder [50] on the horizontal surface between both V-tails enables the aircraft to change the generated lift of the upper wing without creating downforce. This is used to on the one hand trim the aircraft in the most efficient way but also acts as elevator. The DEP system enables CHARGE to create yaw movement by inducing an intentional imbalance in thrust. This differential thrust is more efficient than rudder movement [26]. For large pitch and yaw adjustments and for redundancy reasons the V-tail of CHARGE is also equipped with conventional rudder surfaces. The main function of the V-tail though is to support the structure of the BW while acting as the vertical and horizontal stabiliser. The V-tail has a projected horizontal area of 17.4 m^2 and a distance between the aerodynamic centre of wing and V-tail of 10.6 m. Thus, a horizontal stabiliser volume of 184.3 m^3 is achieved, 73 % of the reference planes horizontal stabiliser volume.

During descend or deceleration it may be necessary to increase the drag of the aircraft. Therefore both wings of CHARGE are fit with a spoiler system that can be deployed when needed.

During low speed CHARGE profits from the DEP's increased airflow around the wings. However, this effect is not sufficient to fulfil the take-off and landing requirements. Therefore CHARGE is equipped with a high lift system on both wings. This System is a combination of a morphing droop nose and a fowler flap on the trailing edge. While the trailing edge devices are constructed in a traditional way, the morphing droop nose is an aerodynamically efficient way of increasing the maximum lift coefficient of the wing while reducing noise emissions compared to a conventional slat [51]. The structural integration of the system can be effectively realised between the motor nacelles.

The high lift design was conducted so that the required lift coefficients for take-off and landing are achieved while maintaining a minimal shift of the aerodynamic centre of the whole aircraft. To achieve this the lift coefficients of both wings are increased proportionally to the wing area distribution between the wings. It must be ensured that the lift coefficients during take-off and landing are reached at a total aircraft angle of attack (AOA) that does not

exceed the rotational clearance angle of the aircraft. The AOA results from the lift polars in the take-off and landing configuration and the installation angle of the wing. The high lift devices of CHARGE are designed so that the lift coefficients during take-off and landing are achieved at AOA and the clearance of 14° is not neglected.

5.7 Aircraft Balance

The location of the aircraft's COG has a massive influence on its flight mechanical behaviour. Therefore, a detailed analysis of the mass distribution of CHARGE was carried out to position the overall COG 10 % in front of the overall aerodynamic centre to ensure statically stable flight behaviour. Due to the nature of the BW the wing position is not as easy to adjust as on traditional wing concepts, which can make meeting this requirement a challenge. This is mainly due to the upper wing being connected to the tail structure and thus being restricted in its position. While the distance between the wings as well as the whole tail section with the upper wing can be altered to move the aerodynamic centre, other constraints like the battery position between the wings and exit locations also need consideration. The positions of the COG and aerodynamic centre are illustrated in figure 5-13.

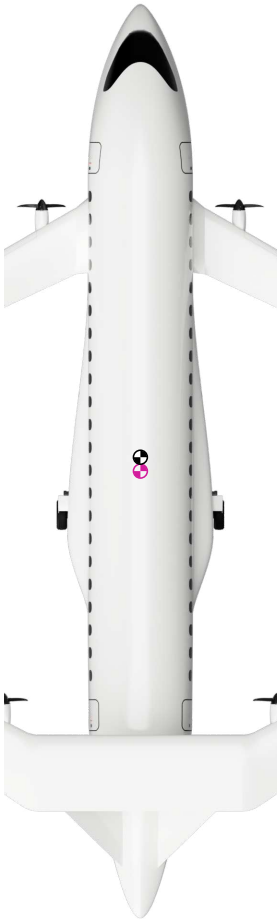

Figure 5-13: Location of COG

Due to the battery mass slightly increasing during flight there is a minor change in COG throughout the mission. However the shift of the COG is only a few centimetres due to the low mass increase and almost symmetrically placement of the batteries around the COG. Therefore, the COG shift can be neglected in flight operations. Same applies for the cabin, as the COG is close to the cabin centre, passengers can be easily placed to prevent a major COG shift for different capacity utilisation. The landing gear is positioned to maintain tilt stability during boarding, deboarding and taxi, but also considering the minimum and maximum nose gear loads.

5.8 Aircraft Performance

To attain a valid design, the propulsion system must provide a certain propulsive power P in all different flight phases and scenarios. This chapter describes how these requirements are formulated for this concept. The results of the calculations provide a design space in terms of take-off wing loading $(G/F)_{\mathrm{TO}}$ within which a valid design can be realised, as seen in figure 5-14. This design space is further constrained by the landing requirements. All power requirements (P/G) are calculated using the methods proposed by Palaia [12]. Due to the lack of public data on thrust characteristics of modern propeller systems, assumptions must be made about the efficiency of the propellers. It is therefore assumed that the efficiency of the propellers is $\eta_{\mathrm{Prop,CR}} = 85\,\%$ in cruise flight and $\eta_{\mathrm{Prop,TO}} = 75\,\%$ during take-off and initial climb. The performance requirements refer to the shaft power of the motors.

The required take-off power is mainly influenced by the Take-Off Field Length (TOFL) and the maximum lift coefficient in takeoff configuration $c_{\mathrm{L,max,TO}}$. Due to the positive influences of DEP, CHARGE is able to perform the take-off in 10 % less distance than a conventional propulsion system design. Consequently, to achieve the demanded TOFL of 1,510 m, less thrust is required. The take-off calculations were made in compliance with CS 25 using methods from Palaia [12] and Sforza [52].
Two scenarios present power requirements for the climb segment. On the one hand, according to CS 25.121, multiple defined climb gradients must be maintained in the event of an engine failure. At the other hand, for normal operations, a climb angle $c_{\mathrm{IC,req}}$ of 4° up to an altitude of 1,000 m must be maintained due to noise avoidance. Above 1.000 m, it is most efficient to climb to cruise altitude as fast as possible to spend the maximum possible time in cruise flight for which the aircraft is designed. This is achieved while climbing with maximum rate of climb (ROC). The ROC and the corresponding airspeed for maximum ROC can be derived from the drag polar of the aircraft and the available thrust expressed as specific excess thrust (SET) and specific excess power (SEP). The optimal airspeed in climb is increasing with altitude. The climb profile of CHARGE is designed to constantly adjust the airspeed to maximum climb speed until the cruise altitude is reached. For the rest of the climb, only 80 % of the available power is used due to the thermal limitations of the engines. The resulting ROC at different altitudes is shown in figure 5-15. All important climb parameters are summarised in table 5-4.

The design cruise altitude H_{CR} for CHARGE is selected so that flights over mountain ranges such as the alps are possible. The operational cruise altitude can however be adapted to each flight mission.

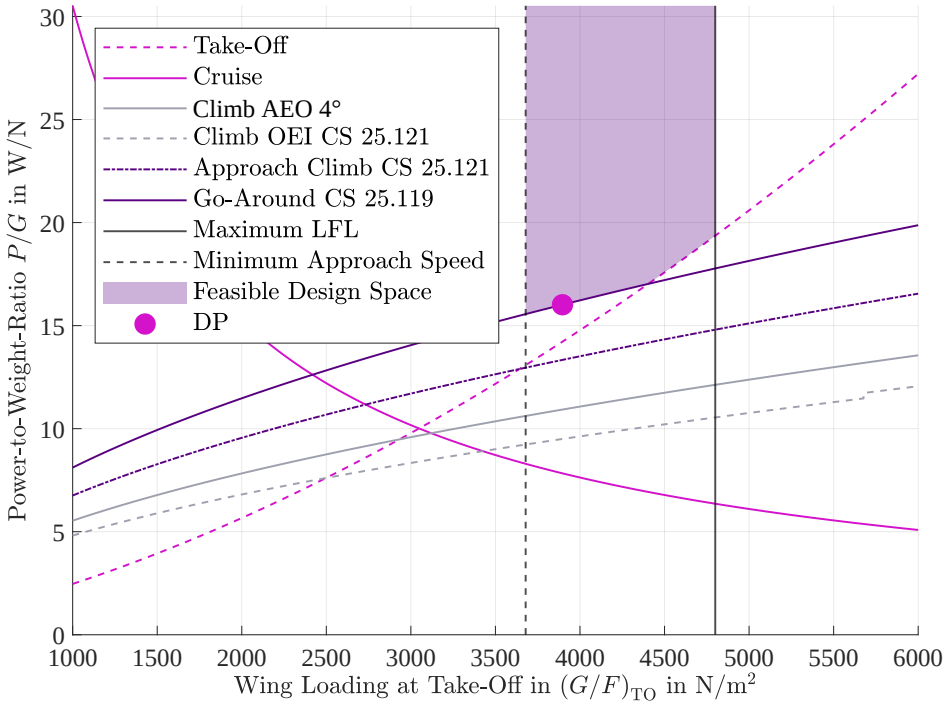

Figure 5-14: Power Requirements as a Function of Wing Loading at Take-off

Table 5-4: Performance Parameters

Parameter	Value
TOFL	1,410 m
$\eta_{\text{Prop,TO}}$	75 %
$C_{\text{L,max,TO}}$	2.2
P_{TO}	5.45 MW
$c_{\text{IC,max}}$	6.6°
mean ROC	6.38 m/s
$\eta_{\text{Prop,CR}}$	85 %
P_{TO}	3.02 MW
mean ROD	6.72 m/s
Descent Profile	Ma 0.57/270 kts IAS
v_{APP}	64.1 m/s
a_{APP}	6.74°
$C_{\text{L,max,LDG}}$	2.8
LFL	1,303 m
s_{LDG}	782 m
$(G/F)_{\text{TO}}$	3,896 N/m²
P_{inst}	6.24 MW

The most efficient descent is conducted at best glide speed $v_{\text{a,min}}$. However, as for CHARGE this flight speed is on average 121 m/s, this would lead to a very long and time consuming descent. For normal operation this is not practical. Therefore CHARGE descends with a predefined profile of Ma 0.57 or 270 kts IAS whichever is lower at given height. Below 10,000 ft the descent speed is reduced to the regulatory maximum of 250 kts IAS. All motors are feathering during descent, thus no energy is used by the propulsion system and the drag is minimised. This compromise ensures both a time and energy efficient descent with the added benefit of reducing noise emissions. The relevant performance data is summarised in table 5-4. Below 1,000 m, again due to noise reducing measures, CHARGE is able to maintain a descent angle of more than 5.5°. This angle is lower than the glide angle a_{APP} which means no additional lift reducing measures like spoilers are necessary to be deployed apart from possible deceleration phases. According to CS 25.119 and CS 25.121 the aircraft has to achieve certain climb gradients in case of an approach climb or go around. This results in additional power requirements that were considered during the design process and are shown in figure 5-14. In terms of wing loading G/F there are two boundaries relevant at landing for the design of CHARGE. The first boundary results from the given maximum landing field length (LFL) of 1,510 m. The required landing distance is mostly influenced by the wing loading and maximum lift coefficient at landing configuration. CHARGE must be able to stop in 60 % of the given maximum LFL. The landing distance is calculated according to Raymer [9]. The other boundary of the wing loading results from a minimal approach speed $v_{\text{APP,min}}$ of International civil aviation organisation (ICAO) approach category C at 121 kts. Any lower approach speed a_{APP} would not be acceptable from an operational perspective. A minimal wing loading can be calculated from the approach speed and maximum lift coefficient in landing configuration $C_{\text{L,max,LDG}}$. Again all the landing parameters and the actual landing distance during normal operation are summarised in table 5-4.

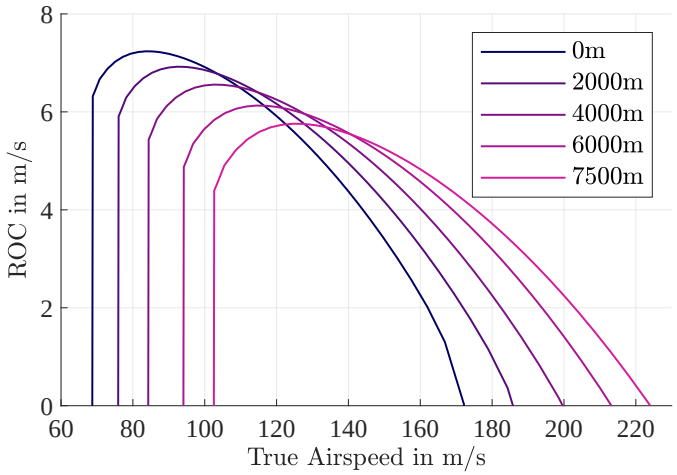

Figure 5-15: ROC at Different Altitudes

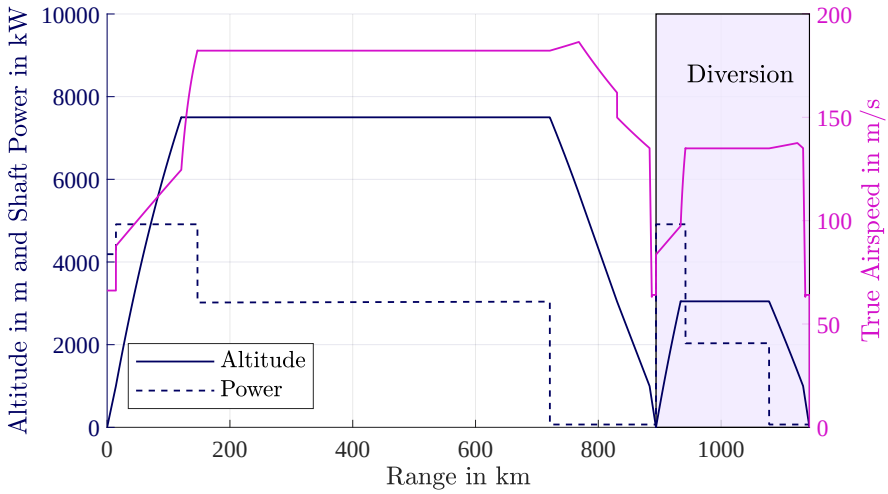

Figure 5-16: Mission Profile for Design Range

Table 5-5: Energy Breakdown

Energy Share		Energy in kW h	% of E_{tot}
E_{trip}	E_{CL}	1,861	25.5
	E_{CR}	2,650	36.3
	E_{des}	24	0.3
	Σ	4,533	62.1
E_{div}		1,278	17.5
E_{HLD}		1,191	16.3
E_{cont}		226	3.1
$E_{sys,misc}$		72	1.0
E_{tot}		7,302	100

With all power requirements and wing loading limits in place a suitable take-off wing loading $(G/F)_{TO}$ can be chosen for the design. Figure 5-14 shows that with increasing wing loading, the required installed power P_{inst} and thus the motor weight also increases. At the same time, the power requirement in cruise flight $(P/G)_{CR}$ decreases, which consequently also leads to an overall lower EC. The wing loading for CHARGE is selected in such a way that a compromise between the two behaviours is formed, taking the resulting wing area A_W and geometry into account looking at the overall design. The take-off wing loading for this design is selected at 3,896 N/m^2 resulting in a required installed power P_{inst} of 6.24 MW. The go-around scenario is dimensioning the thrust for the design as shown in figure 5-14.

To size the battery of CHARGE a detailed analysis of the required energy is necessary. Besides the major energy percentage used by the propulsion group this includes the EC of all aircraft systems. The calculation follows a simple integration of the varying power consumption over the time of the whole flight mission. Besides the trip energy for the mission range E_{trip} and diversion range E_{div}, this includes the energy E_{HLD} for the loitering of 30 min and the contingency energy E_{cont} of 5 % of the trip energy E_{trip}. Figure 5-16 shows the most important flight parameters over the course of the design mission. An additional 1 % of the mission energy is added to the total energy $E_{sys,misc}$ to account for all aircraft systems that were not viewed in detail such as the actuation system and avionics. The total energy E_{tot} amounts to 7.3 MW h and can be divided into the different flight phases according to table 5-5.

6 Airplane Operation and Costs

In this section, the operational characteristics of CHARGE are presented and both the DOC and EC are evaluated. The aircraft is designed not only to optimise flight performance, but also to facilitate operational aspects.

6.1 Operational Concept

To ensure a successful operation on the given flight network, 4 aircraft are required. All aircraft together perform 224 weekly flights with a range between 361 and 894 km and a total of 14 mio. SKO. For the given flight network, an average utilisation of 93% of the passenger capacity and 90 % of the aircraft's possible flighttime is achieved. The individual flight information for the design missions are shown in table 6-1.

CHARGE is equipped with an electric nose landing gear driving system [53]. This speeds up the ground operations and ensures, that taxi in and out times do not exceed the average times given by a report from EUROCONTROL [54]. While the average taxi in time of 4.25 min is already optimised, the average taxi out time of 8.75 min can be further improved with the electric nose landing gear drive system. The aircraft does not need a tug vehicle as it can taxi backwards by itself and can immediately begin to taxi out. In addition, the EC of the electric motor is much lower than when taxiing with the propeller system. The propulsion system can be turned off, once the aircraft has left the runway. This reduces noise at the airport and increases the safety of ground operations because the propulsion system never runs on the ramp. The turnaround process for CHARGE, as illustrated in figure 6-1, demonstrates only little differences from conventional aircraft ground operations, with specific adaptions for a battery electric aircraft.

Table 6-1: Design Missions

Connection	Range in km	Weekly Flights per Direction	Average PAX	Flight Time in min	Trip Energy in MW h	EC in $^{Wh}/_{PAX\,km}$
GOT - VBY	361	7	107	43	2.02	52
HAM - RTM	419	3	76	49	2.14	67
HAM - ANR	464	2	89	55	2.41	58
HAM - GOT	471	10	104	56	2.54	52
HAM - PRG	490	8	103	57	2.62	52
HAM - LUX	517	4	89	60	2.65	58
HAM - MUC	601	12	105	68	3.14	50
HAM - SVG	643	5	100	71	3.29	51
HAM - BGO	795	6	93	85	3.91	53
GOT - UME	808	6	106	87	4.09	48
HAM - EDI	894	9	100	94	4.42	49
HAM - TRF TRF - TRD	478 619	5	109	57 69	2.61 3.26	50 48
HAM - FDH FDH - MRS	578 665	6	98	65 73	2.98 3.37	53 52
HAM - SZG SZG - SJJ	605 683	5	107	68 75	3.17 3.53	49 48
BRI - SZG SZG - HAM	799 683	4	108	86 75	4.07 3.54	47 48

Upon arrival at the ramp the aircraft's integrated stairs are immediately extended. The airstairs are already in use today and represent a reasonable compromise between the extra mass carried and a significant reduction in time spent on the ground [53]. Deboarding begins promptly via the forward stairs, with optional aft stairs provided by the airport to accelerate the process if needed. Simultaneously the ground crew connects the 4 charging plugs, as stated in section 5.2.4, that can charge each battery pack simultaneously. The charging time amounts 12 min to 26 min, depending on the mission range. Lavatory servicing is done concurrently with deboarding, while cabin cleaning starts once deboarding is complete. Boarding is managed through the forward door and optionally through both exits. When the required SOC for the next flight is reached, the ground crew disconnects the charging plugs and the aircraft performs pushback independently using its electric nose gear motor. Despite these elements, the overall turnaround time for most flights is dictated by the traditional procedures rather than the charging time. When charging periods are less than 20 min, common within the network, these times are typically shorter than the conventional turnaround processes, meaning the overall duration of the turnaround remains influenced more by standard operational procedures than by the battery charging itself. For a detailed schematic of the ground operation refer to figure 6-2.

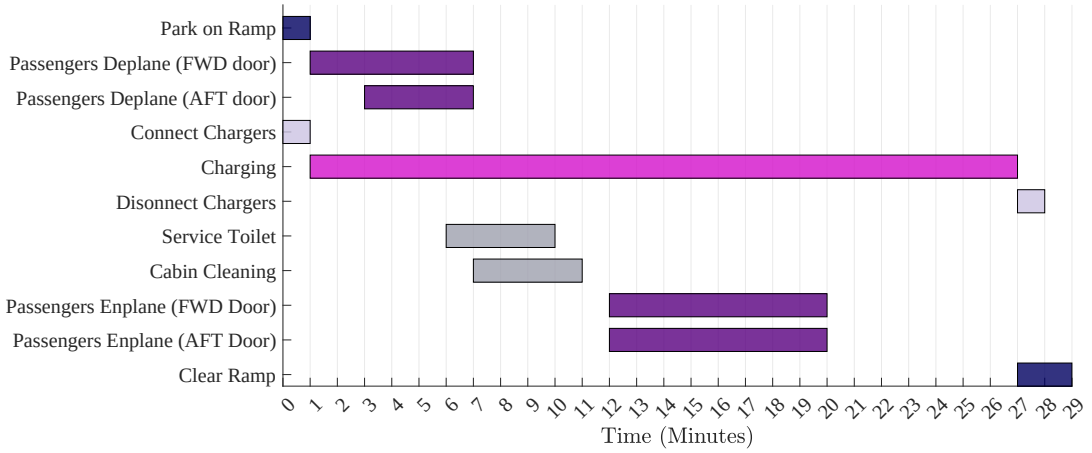

Figure 6-1: Rapid Turnaround Process for CHARGE

As the battery degrades over time, it requires replacement after 1,500 full charging cycles. As the flight network includes shorter ranges and ideally avoids using the reserves, the average flight consumes only 25 % of a full charge cycle. The partial cycle is not calculated from the percentage of the SOC, but rather from the percentage of charging time t_{charge} in comparison to the maximum charging time $t_{\text{charge,full}}$. This ensures a more accurate mapping of the degradation. The cycles are determined as follows:

$$\text{Cycle } [\%] = \frac{t_{\text{charge}}}{t_{\text{charge,full}}} \cdot 100 \qquad \text{(eq 6-1)}$$

Consequently, each battery has an estimated lifespan of 23 months. Two access panels on the starboard side of the plane are used for battery replacement. Changing the batteries can be done during a typical C-check. This ensures minimal disruption to the aircraft's operational availability.

Another operational feature of CHARGE is the single pilot operation system. This can reduce the crew costs by 31%. The cockpit is designed for only one pilot. The pilot can either monitor automated procedures, or steer the aircraft manually. In case of an emergency, it is possible to connect the aircraft to a ground operation station.

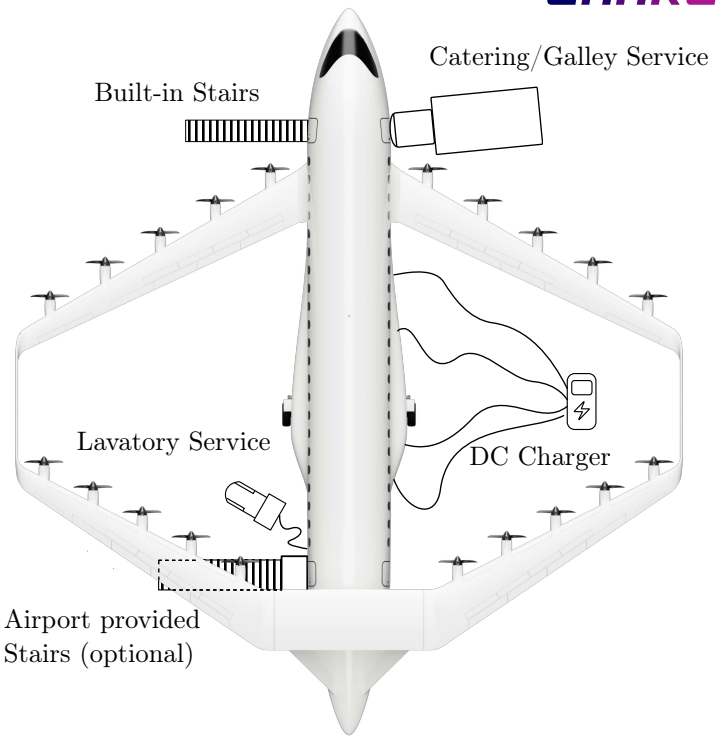

Figure 6-2: Turnaround Schematics

6.2 Payload-Range Diagram

The Payload-Range diagram for CHARGE is shown in figure 6-3. It should be noted that the MLM increases by up to 0.61 t as the range increases. However, the MTOM remains the same with increasing range, as the aircraft always carries the same battery mass. The fixed battery mass prevents a short-term range extension, such as substituting PAX with fuel. Range extensions can only be achieved, if batteries develop higher energy densities during the 20 years of operation or by carrying less PAX. CHARGE has a ferry range of 1,430 km.

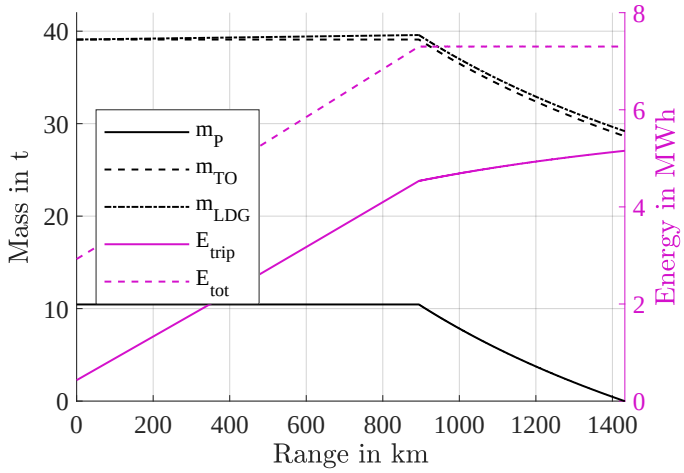

Figure 6-3: Payload-Range Diagram

6.3 Enviromental and Cost Efficiencies

The cost analysis is performed for a period of 20 years using Thorbeck's method [55] and 2019 as a reference year for the $. Due to the unconventional concept, some adjustments need to be made to this method.

As the battery degradation is route dependent, battery costs will be initially added once to the capital costs and subsequently added in percentage to the maintenance costs for each flight. After 1,500 completed cycles of the Li-Air batteries, the required SE is no longer given. The batteries can still be used for numerous second life applications [56]. Thus, the following purchase costs of the batteries are assumed to be 50 % of the initial battery costs of 200 $\$_{2019}/\text{kWh}$. The time between overhaul for electric propulsion systems is 10 times as high as conventional engines, thus the maintenance costs for engines will be reduced by 90% [9]. A single pilot operation enables a 31 % reduction of the crew costs, thus the SKC are reduced by 0.46 $\$_{2019}$ - Cent, appropximately 6%. A breakdown of the DOC for the given network is shown in figure 6-4. CHARGE achieves an average SKC of 7.09 $\$_{2019}$ - Cent and an EC of 50.6 Wh/kg per PAX.

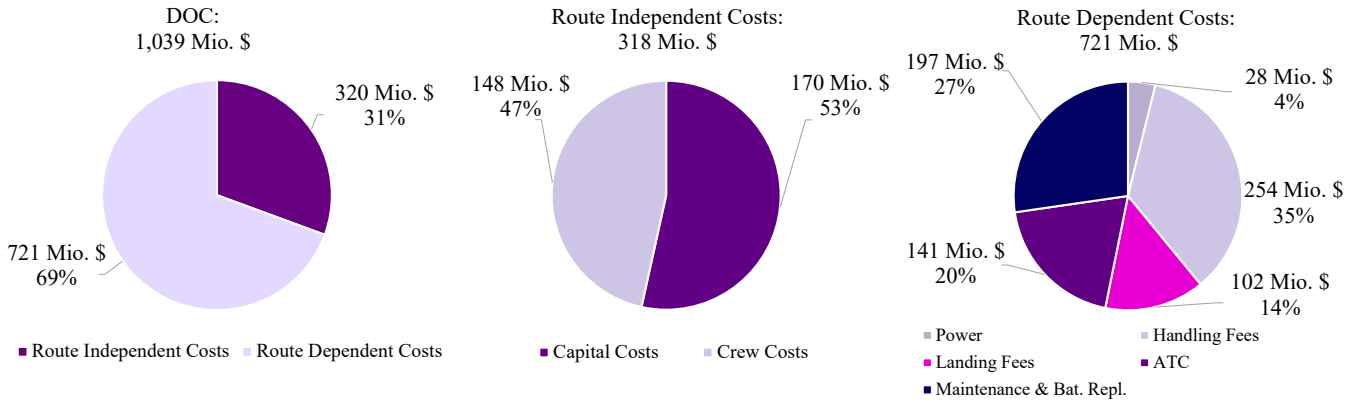

Figure 6-4: Breakdown of DOC for Operational Time of 20 Years

Figure 6-5 shows the SKC and EC for CHARGE compared to the Dash 8 [57]. The DOC and EC are shown for fully loaded aircraft as a function of the range. The marked points show CHARGE's performance for the average network given, they are slightly higher due to lower utilisation.

CHARGE achieves up to 20 % lower SKC on the given network and consumes 80 % less than Dash 8's energy. However, the comparison should be treated with caution, as kerosene and energy consumption can only be compared with the lower heating value for SAF of 43.2171 $^{MJ}/_{kg}$. When comparing costs, it should be noted that the Dash 8 has a longer design range than CHARGE, although the Dash 8 is known to fly short distances. The table 8-2 compares the performance of CHARGE and the Dash 8.

The costs for energy are impressively low, compared to fuel costs for similar sized aircraft. The price per kWh for electricity of 0.038 $\$_{2019}$ in 2050 is expected to be significantly lower than for SAF with 0.104 $\$_{2019}$, additionally the grid to shaft efficiency is more than 5 times higher as shown in table 3-1. The maintenance costs for CHARGE are approximately 150 Mio. $\$_{2019}$ lower than for the Dash 8, due to the electric propulsion. The reduced maintenance and energy costs of CHARGE, both of which depend on the route, combined with the reduced crew costs, result in CHARGE being more economical to operate, even though the initial capital cost is relatively high.

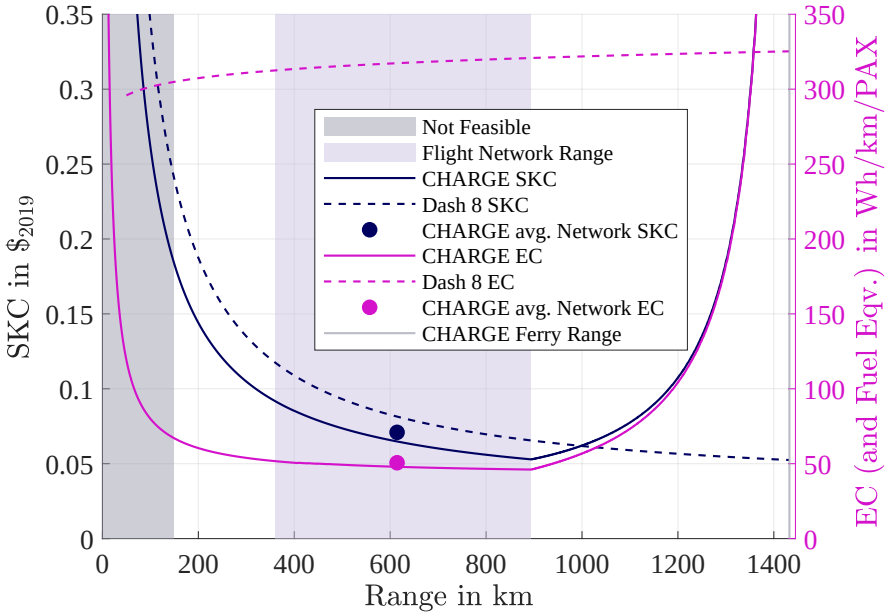

Figure 6-5: SKC and EC for CHARGE and Dash 8

7 Iteration and Optimisation

In this years design challenge the assignment is to design an aircraft to operate on a given network in the most efficient way possible taking cost and energy usage into account. In order to fulfil this assignment, it was necessary to set up an iterative design loop to estimate the costs of different abreast and PAX configurations for both direct and indirect route networks. As a consequence, the iterative design loop was used to create not only a single configuration of CHARGE, but also multiple valid configurations and calculate the energy usage and operating costs for the given route network. This can be seen on diagram 3-3, where all the calculated configurations for both indirect and direct flights are evaluated to identify the optimal solution in accordance with the selected optimising factors for energy and costs.

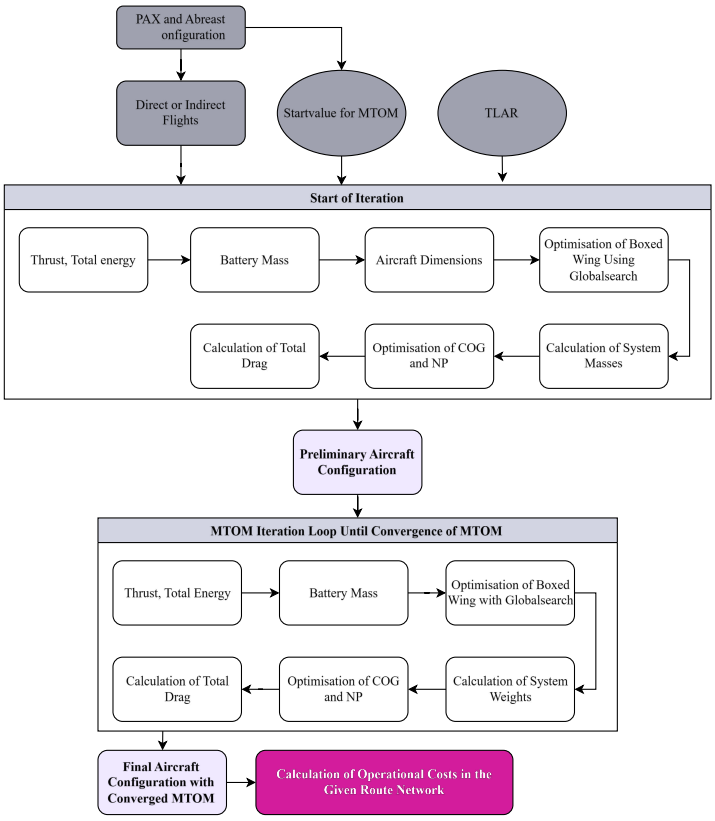

Figure 7-1: Diagram of the MATLAB Iteration Loop

As shown in figure 7-1, the calculation of the aircraft configuration contains two main steps. Firstly, the preliminary configuration is calculated with the input values for the initial MTOM, the cabin configuration and top level aircraft requirements (TLAR). In this step, the geometry of the wing is thoroughly optimised using the "globalsearch" algorithm to change all the parameters of the wing in a predefined range. In the second step of the iteration the same steps are calculated as before until the MTOM value has converged. In this step, the wing optimisation is less complex and the wing is only scaled to accommodate the change in MTOM and the horizontal stagger is adjusted to optimise the location of the wing.

Once a valid configuration has reached the end of the optimisation algorithm the DOC and EC are calculated based on either the direct and indirect route network selected at the beginning. These values serve a basis for the scoring calculation and the figure 3-3.

8 Discussion and Conclusion

In the previous sctions, a number of arguments were presented in favour of the proposition that CHARGE represents an optimal solution for carbon neutral regional electric flight. In the following chapter, the feasibility of the concept is evaluated. Furthermore, certain technologies that may require further investigation before they can be considered ready for use are identified. The key aspects of CHARGE are compared to the reference aircraft's, followed by a final conclusion.

8.1 Technology Readiness Level and Further Investigations

It is essential to evaluate the technologies used in CHARGE in terms of their current and projected technological maturity and to identify research needs. The Technology Readiness Level (TRL) is a method for estimating the maturity of technology during the planning phase of a project to deliver a consistent and uniform statement for the concepts feasibility. It is defined by the Deutsches Institut für Normung (DIN) Europa Norm (EN) 16603-11 standard. The levels reach from TRL 1 for "Basic principles observed" up to TRL 9 for "Actual system proven in operational environment" [58]. In the context of this paper all crucial technologies are rated by this standard. Table 8-1 displays a list of the most innovative and critical technologies used for CHARGE.

It is not possible to make a general statement about the speed of development, as all technologies progress at different rates. Therefore, it does not make sense to require a certain current TRL for CHARGE, but to evaluate each technology separately. According to the research done, all technologies used for CHARGE will have

a TRL of at least 8 in 2050. As shown in table 8-1, further research and design work is necessary for a concept like CHARGE to take to the skies by 2050. The key technologies and topics that need the most research effort are the Li-Air batteries, the aerodynamic properties of a BW with DEP and high voltage power distribution in combination with high efficient motors and power electronics.

Table 8-1: TRL for Relevant Technologies for the Concept

Technology	TRL	Source
E-Taxi	8-9	[53]
Box Wing	5	[59]
MMEI	4	[60]
High Voltage Power Distribution	2-3	[61]
Motor & Inverter	3	[62]
DEP	3	[63]
Battery	2-3	[64]
Sandwich structure	4	[65]
Electric ECS	9	[66]
Integrated TMS ECS	6	[67, 44]
Morphing Trim Section	4	[50, 68]
Morphing Droop Nose	4	[51]
Single Pilot Operations	5	[69]

The Li-Air batteries can be seen as the most important key technology not only for CHARGE, but for a more environmentally friendly aviation and transport sector in general. Currently the chemical reaction of these batteries has been researched and the first prototypes in laboratories have been tested. Further research is definitely required into to mass production of such batteries and their durability during the life cycle. Also the safety aspects like methods to extinguish the batteries need to be investigated further. Lithium mining poses a number of challenges that will need to be addressed in the future. Care must be taken in ensuring that mining is environmentally friendly and fair, to avoid excessive water consumption and exploitation of nature. This ensures that CHARGE is not only carbon neutral, but also environmentally friendly in general. Nevertheless trends in research show that in the given time frame until 2050 is sufficient for this technology to reach market maturity [64].

The aerodynamic properties of a BW and DEP require further investigations not only to research the effects on flight dynamics of such a design, but also to find further ways to increase the efficiency through extensive analysis of the aeropropulsive interaction. Since, in addition to widespread theoretical research, test platforms for DEP are already being operated [63] and box wing concepts are analysed in wind tunnel experiments [70, 71], it is assumed that this technology will be mature and reaching the desired efficiency improvements to be operational by 2050.

A further topic of relevance to the BW aircraft is the structural concept for the application of loads from the upper wing and the integration into fuselage via the V-tail. While this concept appears to offer a logical solution from a basic mechanical standpoint, further investigation is required to fully assess its viability.

High voltage power distribution paired with high efficiency motor and power electronics technology is another topic relevant not only to CHARGE, but also to other more and all electric concepts. As aircraft might start incorporating hybrid powertrains, such power distribution systems and their limits become relevant to achieve an efficient and safe design. Intensive research in this area [72, 73, 62], but also already conducted component tests [74] suggest that the speed of development of these technologies will be high enough to be commercially viable by 2050. In addition to the technology itself, the progress in regulations to operate such systems also has a crucial impact, but this is already being addressed today [75].

The ECS is of vital importance for civil airliners operating at altitudes above 8,000 ft, as it provides passengers with oxygen-enhanced, pressurised and heated air. The TMS, on the other hand, is responsible for cooling essential electrical components, such as the aircraft's batteries. By utilising a heat exchanger, the cold ambient air can be heated by the batteries, thereby cooling them down while simultaneously heating the cabin or WIPS. This process renders the ECS obsolete. Even though this technology is, on a basic level, already applied in aircraft like the Airbus A350 and Boeing B787, there is further investigation required to apply the for CHARGE in the proposed way.

Nowadays the implementation of a single pilot cockpit is not authorised according to CS-25. In the future, this presents the potential for cost optimisation without any compromise. In order to ensure the safety of the aircraft operation and thus obtain the necessary certification, further research is required. The European Union Aviation Safety Agency (EASA) plans to enable commercial flights with single pilot operations by 2030 [76], which translates into availability when CHARGE enters service.

8.2 Comparison of Key Specifications to Reference Aircraft

The Dash 8 was chosen as a comparison aircraft as it is a popular choice on regional networks. Considering technical aspects listed in table 8-2 the Dash 8 has similarities to CHARGE as it is powered by propeller engines, can carry a similar PAX amount, has an almost equal wingspan and a slightly higher H_{CR} and Ma_{CR}. CHARGE can carry 20 more PAX with an approximately 6 times lower EC. The maximum range R_{max} of CHARGE is considerably lower than the Dash 8's, but CHARGE is optimised to operate on a defined route network.

Table 8-2: Comparison between CHARGE and Dash 8

Value	Unit	CHARGE	Dash 8
Average ROC	$^{m}/_{s}$	6.36	9.16
Total Energy E_{tot}	MW h	7.11	25.70
Cruise Mach Number Ma_{CR}	1	0.57	0.60
Cruise Altitude H_{CR}	m	7,500	7,620
Wing Span b	m	28	28.4
Wing Area F	m^2	98.4	54.4
Take-Off Wing Loading $^{G}/_{F}$	$^{N}/_{m^2}$	3,868	4,349
Length	m	30.5	32.8
MTOM	t	39.1	30.5
PAX	1	110	90
Abreast	1	5	4
DOC for 20 Years, 4 Aircraft	Mio. $\$_{2019}$	1,039	1,176
Capital Costs per Aircraft	Mio. $\$_{2019}$	42.55	34.04
SKC	$\$_{2019}$	7.09	8.03
EC	$^{W h}/_{PAX km}$	50.64	320.31
Design Range	km	894	2,040
TOFL	m	1,410	1,300
LFL	m	1,303	1,100

8.3 Conclusion

As demonstrated in preceding sections, electricity represents the optimal source of power for an aircraft engaged in short-haul operations. Although battery technology is not yet sufficiently advanced to enable the production of fully electric aircraft, it is likely to be adequately advanced by an EIS in 2050. This will provide another potential avenue for future development. It is unlikely that alternative technologies such as SAF or hydrogen-powered aircraft will ever be able to fly beyond their initial design range, whereas CHARGE will be able to fly further as soon as battery technology improves. Another benefit of a fully electric aircraft is the reduced environmental impact and economic cost as, electricity is a more cost-effective option compared to SAF or hydrogen alternatives. The selected Li-Air Batteries are straightforward to integrate into the aircraft system and promise comparable safety profiles to conventional lithium-ion batteries, given the absence of self-inflammation. If all provided power is generated in an emission-free manner, CHARGE's operation will be entirely carbon neutral. Given that turnaround times at airports can be reduced to a finite limit, as discussed in chapter 6, the charging time is not a significant factor in this concept. This allows for the seamless integration of aircraft into airline fleets and the operation of planes on regional routes.

The chosen BW configuration, in combination with the DEP enables a quiet and efficient flight for regional and domestic operations. Furthermore, the wing area is divided into two smaller sections instead of one large one, resulting in a notable reduction in the dimensions of CHARGE and enhanced operational suitability at smaller regional airports. To reduce turnaround time at airports and thus decrease operational costs for the airline, as well as provide independence from airport infrastructure, the motor, built into the front gear, plays an important role. The numerous small propellers provide a consistent airflow around the wings, thereby enhancing take-off performance and resulting in a noticeably shorter take-off distance than that of the comparable Dash 8. Moreover, the highly efficient electric system and the efficient grid-to-shaft ratio of electricity, as illustrated in table 3-1, contribute to the aircraft's capacity to attain an extremely low EC. A substantial contribution to the realisation of this performance is made by the selected motors, powering the propellers, which have been the subject of comprehensive research at NASA and are capable of achieving efficiencies in excess of 99 %. This enables CHARGE to achieve a tank-to-shaft efficiency of over 93 %.

In conclusion, it can be stated that an electric aircraft like CHARGE represents the optimal solution for regional and short-haul flights, while satisfying all required performance parameters. It is more climate friendly and, despite its innovative nature, is still more cost-effective to operate than other comparable state-of-the-art aircraft.

So get ready and CHARGE up! Because the future of regional flight is electric and about to become reality.

References

[1] *Mehr als die Hälfte aller Passagierflüge in Deutschland waren 2020 Kurzstreckenflüge*. Statistisches Bundesamt. URL: https://www.destatis.de/DE/Presse/Pressemitteilungen/2021/06/PD21_N037_46.html (visited on 07/15/2024).

[2] Hannah Ritchie and Max Roser. "What share of global CO2 emissions come from aviation?" In: *Our World in Data* (Apr. 8, 2024). URL: https://ourworldindata.org/global-aviation-emissions (visited on 07/15/2024).

[3] Reynard de Vries et al. "A New Perspective on Battery-Electric Aviation, Part II: Conceptual Design of a 90-Seater". In: Jan. 4, 2024. DOI: 10.2514/6.2024-1490.

[4] Giuseppe Palaia, Karim Abu Salem, and Alessandro A. Quarta. "Comparative Analysis of Hybrid-Electric Regional Aircraft with Tube-and-Wing and Box-Wing Airframes: A Performance Study". In: *Applied Sciences* 13.13 (Jan. 2023). Number: 13, p. 7894. ISSN: 2076-3417. DOI: 10.3390/app13137894. URL: https://www.mdpi.com/2076-3417/13/13/7894 (visited on 04/08/2024).

[5] Karim Abu Salem, Giuseppe Palaia, and Alessandro Antonio Quarta. "Introducing the Box-Wing Airframe for Hybrid-Electric Regional Aircraft: A Preliminary Impact Assessment". In: *Applied Sciences* 13.18 (Jan. 2023). Number: 18, p. 10506. ISSN: 2076-3417. DOI: 10.3390/app131810506. URL: https://www.mdpi.com/2076-3417/13/18/10506 (visited on 04/08/2024).

[6] Daniel Schiktanz. "Conceptual Design of a Medium Range Box Wing Aircraft". Master Thesis. Hochschule für Angewandte Wissenschaften Hamburg, 2011.

[7] Finck, R. D. *USAF (United States Air Force) Stability and Control DATCOM (Data Compendium)*. Apr. 1, 1978. URL: https://apps.dtic.mil/sti/citations/ADB072483 (visited on 07/07/2024).

[8] Fanklin W. Diederich. *A simple approximate method for calculating spanwise lift distributions and aerodynamic influence coefficients*. Aug. 1, 1952. URL: https://ntrs.nasa.gov/citations/19930083506 (visited on 07/07/2024).

[9] Daniel P. Raymer. *Aircraft design: a conceptual approach*. AIAA education series. Reston, VA: American Institute of Aeronautics and Astronautics, Inc, 2018. ISBN: 978-1-62410-490-9.

[10] Egbert Torenbeek. *Synthesis of Subsonic Airplane Design*. Dordrecht: Springer Netherlands, 1982. ISBN: 978-90-481-8273-2. DOI: 10.1007/978-94-017-3202-4.

[11] Leland M. Nicolai and Grant Carichner. *Fundamentals of aircraft and airship design*. AIAA educational series. Reston, VA: American Institute of Aeronautics and Astronautics, 2010. ISBN: 978-1-60086-751-4.

[12] Giuseppe Palaia. "Design and performance assessment methodologies for box-wing hybrid-electric aircraft from urban to regional transport applications". PhD thesis. Pisa: Università di Pisa.

[13] Martin Hepperle. "Aspects of Distributed Propulsion". Oct. 5, 2016.

[14] G. Girishkumar et al. "Lithium-Air Battery: Promise and Challenges". In: *The Journal of Physical Chemistry Letters* 1.14 (July 15, 2010). Publisher: American Chemical Society, pp. 2193–2203. DOI: 10.1021/jz1005384. URL: https://doi.org/10.1021/jz1005384 (visited on 04/25/2024).

[15] Smruti Sahoo, Xin Zhao, and Konstantinos Kyprianidis. "A Review of Concepts, Benefits, and Challenges for Future Electrical Propulsion-Based Aircraft". In: *Aerospace* 7.4 (Apr. 2020). Number: 4 Publisher: Multidisciplinary Digital Publishing Institute, p. 44. ISSN: 2226-4310. DOI: 10.3390/aerospace7040044. URL: https://www.mdpi.com/2226-4310/7/4/44 (visited on 06/17/2024).

[16] Md. Arafat Rahman, Xiaojian Wang, and Cuie Wen. "A review of high energy density lithium–air battery technology". In: *Journal of Applied Electrochemistry* 44.1 (Jan. 1, 2014), pp. 5–22. ISSN: 1572-8838. DOI: 10.1007/s10800-013-0620-8. URL: https://doi.org/10.1007/s10800-013-0620-8 (visited on 06/13/2024).

[17] AIRBUS. "Global Market Forecast 2023". Toulouse, June 13, 2023. (Visited on 07/15/2023).

[18] Juliane Bopst et al. "Wohin geht die Reise? Luftverkehr der Zukunft: umwelt- und klimaschonend, treibhausgasneutral, lärmarm". In: *Umweltbundesamt* (Nov. 2019). ISSN: 2363-832X. (Visited on 07/12/2024).

[19] *ReFuelEU Aviation - European Commission*. URL: https://transport.ec.europa.eu/transport-modes/air/environment/refueleu-aviation_en (visited on 07/07/2024).

[20] *Regulation (EU) 2023/2405 of the European Parliament and of the Council of 18 October 2023 on ensuring a level playing field for sustainable air transport (ReFuelEU Aviation)*. Legislative Body: CONSIL, EP. Oct. 18, 2023. URL: http://data.europa.eu/eli/reg/2023/2405/oj/eng (visited on 07/08/2024).

[21] *Global Energy Transition A Roadmap to 2050*. Table 1. Apr. 16, 2018, p. 30. URL: https://www.irena.org/publications/2018/Apr/Global-Energy-Transition-A-Roadmap-to-2050 (visited on 07/08/2024).

[22] Alex Schmitt. *EU Energy Outlook 2050: How will the European electricity market develop over the next 30 years?* Energy BrainBlog. Apr. 11, 2022. URL: https://blog.energybrainpool.com/en/eu-energy-outlook-

2050-how-will-the-european-electricity-market-develop-over-the-next-30-years/ (visited on 07/08/2024).
[23] *Lilium*. URL: https://jet.lilium.com/ (visited on 07/17/2024).
[24] *X-57 Maxwell Overview - NASA*. Section: Armstrong Flight Research Center. Sept. 13, 2018. URL: https://www.nasa.gov/centers-and-facilities/armstrong/x-57-maxwell/ (visited on 07/17/2024).
[25] Michal Janovec et al. "Performance and Weight Parameters Calculation for Hydrogen- and Battery-Powered Aircraft Concepts". In: *Aerospace* 10.5 (May 2023). Number: 5 Publisher: Multidisciplinary Digital Publishing Institute, p. 482. ISSN: 2226-4310. DOI: 10.3390/aerospace10050482. URL: https://www.mdpi.com/2226-4310/10/5/482 (visited on 04/03/2024).
[26] Martin Hepperle. "Electric Flight - Potential and Limitations". In: AVT-209 Workshop on ENERGY EFFICIENT TECHNOLOGIES AND CONCEPTS OPERATION. Oct. 22, 2012. URL: https://www.researchgate.net/publication/234738753_Electric_Flight_-_Potential_and_Limitations.
[27] L. Prandtl. *Induced drag of multiplanes*. NTRS Author Affiliations: NTRS Report/Patent Number: NACA-TN-182 NTRS Document ID: 19930080964 NTRS Research Center: Legacy CDMS (CDMS). Feb. 1, 1924. URL: https://ntrs.nasa.gov/citations/19930080964 (visited on 07/11/2024).
[28] *ICAO Aerodrome Reference Code | SKYbrary Aviation Safety*. URL: https://skybrary.aero/articles/icao-aerodrome-reference-code (visited on 07/11/2024).
[29] Majid T. Fard et al. "Aircraft Distributed Electric Propulsion Technologies—A Review". In: *IEEE Transactions on Transportation Electrification* 8.4 (Dec. 2022). Conference Name: IEEE Transactions on Transportation Electrification, pp. 4067–4090. ISSN: 2332-7782. DOI: 10.1109/TTE.2022.3197332. URL: https://ieeexplore.ieee.org/document/9852268 (visited on 07/07/2024).
[30] *EASA.P.002 - Dowty R 408 series propellers | EASA*. URL: https://www.easa.europa.eu/en/document-library/type-certificates/propeller-cs-p/easap002-dowty-r-408-series-propellers (visited on 07/15/2024).
[31] *EASA.IM.E.049 - Pratt & Whitney Canada PW150 series | EASA*. URL: https://www.easa.europa.eu/en/document-library/type-certificates/engine-cs-e/easaime049-pratt-whitney-canada-pw150-series (visited on 07/15/2024).
[32] Kevin R. Moore and Andrew Ning. "Takeoff and Performance Trade-Offs of Retrofit Distributed Electric Propulsion for Urban Transport". In: *Journal of Aircraft* 56.5 (2019). Publisher: American Institute of Aeronautics and Astronautics _eprint: https://doi.org/10.2514/1.C035321, pp. 1880–1892. ISSN: 0021-8669. DOI: 10.2514/1.C035321. URL: https://doi.org/10.2514/1.C035321 (visited on 07/08/2024).
[33] Ralph H. Jansen et al. "High Efficiency Megawatt Motor Conceptual Design". In: AIAA Propulsion and Energy Forum and Exposition (AIAA Propulsion and Energy 2018). Cincinnati, OH, July 10, 2018. URL: https://ntrs.nasa.gov/citations/20190030477 (visited on 04/11/2024).
[34] Matthew G. Granger et al. "Concept Design a 1.4 MW Inverter for Rotor Loss Minimization in a Partially Superconducting Motor". In: 2022 IEEE/AIAA Transportation Electrification Conference and Electric Aircraft Technologies Symposium (ITEC+EATS). Anaheim, CA. URL: https://ntrs.nasa.gov/citations/20220006082 (visited on 07/10/2024).
[35] Mona Ghassemi, Ashkan Barzkar, and Mohammadreza Saghafi. "All-Electric NASA N3-X Aircraft Electric Power Systems". In: *IEEE Transactions on Transportation Electrification* 8.4 (Dec. 2022). Conference Name: IEEE Transactions on Transportation Electrification, pp. 4091–4104. ISSN: 2332-7782. DOI: 10.1109/TTE.2022.3158186. URL: https://ieeexplore.ieee.org/document/9730878 (visited on 06/14/2024).
[36] Patrick C. Vratny, Holger Kuhn, and Mirko Hornung. "Influences of voltage variations on electric power architectures for hybrid electric aircraft". In: *CEAS Aeronautical Journal* 8.1 (Mar. 1, 2017), pp. 31–43. ISSN: 1869-5590. DOI: 10.1007/s13272-016-0218-z. URL: https://doi.org/10.1007/s13272-016-0218-z (visited on 06/17/2024).
[37] Ashkan Barzkar and Mona Ghassemi. "Electric Power Systems in More and All Electric Aircraft: A Review". In: *IEEE Access* 8 (2020). Conference Name: IEEE Access, pp. 169314–169332. ISSN: 2169-3536. DOI: 10.1109/ACCESS.2020.3024168. URL: https://ieeexplore.ieee.org/document/9197600 (visited on 07/11/2024).
[38] Angel Recalde et al. "Optimal Voltage for More Electric Aircraft direct current cabling system". In: *2021 IEEE Transportation Electrification Conference & Expo (ITEC)*. 2021 IEEE Transportation Electrification Conference & Expo (ITEC). ISSN: 2377-5483. June 2021, pp. 106–111. DOI: 10.1109/ITEC51675.2021.9490090. URL: https://ieeexplore.ieee.org/document/9490090 (visited on 06/18/2024).
[39] Andrew A. Woodworth, E. Eugene Shin, and Maricela Lizcano. "High Voltage Insulation for Electrified Aircraft". Oct. 22, 2018. URL: https://ntrs.nasa.gov/citations/20190001912 (visited on 07/11/2024).

[40] David C. Loder, Andrew Bollman, and Michael J. Armstrong. "Turbo-electric Distributed Aircraft Propulsion: Microgrid Architecture and Evaluation for ECO-150". In: *2018 IEEE Transportation Electrification Conference and Expo (ITEC)*. 2018 IEEE Transportation Electrification Conference and Expo (ITEC). June 2018, pp. 550–557. DOI: 10.1109/ITEC.2018.8450180. URL: https://ieeexplore.ieee.org/document/8450180 (visited on 07/12/2024).

[41] DIN Deutsches Institut für Normung e. V., ed. *DIN EN 2853 Luft- und Raumfahrt – Strombelastbarkeit von elektrischen Leitungen mit Leiter nach EN 2083; Deutsche und Englische Fassung EN 2853:2005*. Oct. 2006.

[42] Venkatasubramanian Viswanathan et al. "The challenges and opportunities of battery-powered flight". In: *Nature* 601.7894 (Jan. 2022). Number: 7894 Publisher: Nature Publishing Group, pp. 519–525. ISSN: 1476-4687. DOI: 10.1038/s41586-021-04139-1. URL: https://www.nature.com/articles/s41586-021-04139-1 (visited on 03/29/2024).

[43] Xuanxuan Bi et al. "Rechargeable Zinc–Air versus Lithium–Air Battery: from Fundamental Promises Toward Technological Potentials". In: *Advanced Energy Materials* 14.6 (2024). _eprint: https://onlinelibrary.wiley.com/doi/pdf/10.1002/aenm.202302388, p. 2302388. ISSN: 1614-6840. DOI: 10.1002/aenm.202302388. URL: https://onlinelibrary.wiley.com/doi/abs/10.1002/aenm.202302388 (visited on 04/25/2024).

[44] Y. Wang et al. "Energy optimization of aircraft thermal management system". In: *CSAA/IET International Conference on Aircraft Utility Systems (AUS 2022)*. CSAA/IET International Conference on Aircraft Utility Systems (AUS 2022). Vol. 2022. Aug. 2022, pp. 1271–1277. DOI: 10.1049/icp.2022.1856. URL: https://ieeexplore.ieee.org/abstract/document/9946293 (visited on 06/17/2024).

[45] Victor Cavalcanti and Claudia Andrade. "A Trade-off Study of a Bleedless and Conventional Air Conditioning Systems". In: Oct. 7, 2008. DOI: 10.4271/2008-36-0001.

[46] Jonathan M. Rheaume, Malcolm Macdonald, and Charles E. Lents. "Commercial Hybrid Electric Aircraft Thermal Management System Design, Simulation, and Operation Improvements". In: *2019 AIAA/IEEE Electric Aircraft Technologies Symposium (EATS)*. 2019 AIAA/IEEE Electric Aircraft Technologies Symposium (EATS). Aug. 2019, pp. 1–23. DOI: 10.2514/6.2019-4492. URL: https://ieeexplore.ieee.org/document/8941414 (visited on 07/12/2024).

[47] Jeffryes W. Chapman, Hashmatullah Hasseeb, and Sydney Schnulo. "Thermal Management System Design for Electrified Aircraft Propulsion Concepts". In: *2020 AIAA/IEEE Electric Aircraft Technologies Symposium (EATS)*. 2020 AIAA/IEEE Electric Aircraft Technologies Symposium (EATS). Aug. 2020, pp. 1–23. URL: https://ieeexplore.ieee.org/document/9235177 (visited on 06/17/2024).

[48] D Schiktanz and D Scholz. "Box Wing Fundamentals - an Aircraft Design Perspective". In: (2011).

[49] Emanuele Rizzo. *Optimization Methods Applied to the preliminary design of innovative non conventional aircraft configurations*. Google-Books-ID: bSCv_8FIOFMC. Emanuele Rizzo, 2009. 172 pp. ISBN: 978-88-467-2458-8.

[50] A Wildschek, T Havar, and K Plötner. "An all-composite, all-electric, morphing trailing edge device for flight control on a blended-wing-body airliner". In: *Proceedings of the Institution of Mechanical Engineers, Part G: Journal of Aerospace Engineering* 224.1 (Jan. 1, 2010). Publisher: IMECHE, pp. 1–9. ISSN: 0954-4100. DOI: 10.1243/09544100JAERO622. URL: https://doi.org/10.1243/09544100JAERO622 (visited on 07/19/2024).

[51] Srinivas Vasista et al. "Morphing Wing Droop Nose with Large Deformation: Ground Tests and Lessons Learned". In: *Aerospace* 6.10 (Oct. 2019). Number: 10 Publisher: Multidisciplinary Digital Publishing Institute, p. 111. ISSN: 2226-4310. DOI: 10.3390/aerospace6100111. URL: https://www.mdpi.com/2226-4310/6/10/111 (visited on 06/21/2024).

[52] Pasquale M. Sforza. *Commercial Airplane Design Principles*. 1st ed. Oxford: Elsevier Inc., 2014. ISBN: 978-0-12-419953-8.

[53] F Gomez and D Scholz. "IMPROVEMENTS TO GROUND HANDLING OPERATIONS AND THEIR BENEFITS TO DIRECT OPERATING COSTS". In: (2009).

[54] *Taxi times - Winter 2021-2022 | EUROCONTROL*. May 9, 2022. URL: https://www.eurocontrol.int/publication/taxi-times-winter-2021-2022 (visited on 07/15/2024).

[55] J Thorbeck. *TU Berlin - Simplified DOC model*. In collab. with D. Scholz. Sept. 19, 2013.

[56] Jia Woon Lee et al. "Technical feasibility and economics of repurposed electric vehicles batteries for power peak shaving". In: *Journal of Energy Storage* 40 (Aug. 1, 2021), p. 102752. ISSN: 2352-152X. DOI: 10.1016/j.est.2021.102752. URL: https://www.sciencedirect.com/science/article/pii/S2352152X21004825 (visited on 07/19/2024).

[57] *Institut für Luft- und Raumfahrt*. URL: https://luftbau.ilr.tu-berlin.de/webapps/#app/directOperatingCosts (visited on 07/15/2024).

[58] DIN-Normenausschuss Luft- und Raumfahrt (NL) and Aerospace Standards Committee. *DIN EN 16603-11: Space engineering - Definition of the Technology Readiness Levels (TRLs) and their criteria of assessment (ISO 16290:2013, modified)*. Ed. by DIN Deutsches Institut für Normung e. V. Feb. 2020.

[59] None. *Jane's all the world's aircraft, 1987-88*. In collab. with Internet Archive. London ; New York : Jane's, 1987. 1100 pp. ISBN: 978-0-7106-0850-5.

[60] E. Eugene Shin. "Feasibility of Micro-Multilayer Multifunctional Electrical Insulation (MMEI) System for High Voltage Applications". URL: https://ntrs.nasa.gov/citations/20230006503 (visited on 07/19/2024).

[61] Ashkan Barzkar and Mona Ghassemi. "Components of Electrical Power Systems in More and All-Electric Aircraft: A Review". In: *IEEE Transactions on Transportation Electrification* 8.4 (Dec. 2022). Conference Name: IEEE Transactions on Transportation Electrification, pp. 4037–4053. ISSN: 2332-7782. DOI: 10.1109/TTE.2022.3174362. URL: https://ieeexplore.ieee.org/abstract/document/9772493 (visited on 06/14/2024).

[62] *High-Efficiency Megawatt Motor (HEMM)*. Glenn Research Center | NASA. Apr. 11, 2024. URL: https://www1.grc.nasa.gov/aeronautics/eap/technology/hemm/ (visited on 04/11/2024).

[63] *De-risking the key technology distributed electric*. URL: https://clean-aviation.eu/de-risking-the-key-technology-distributed-electric-propulsion-using-the-scaled-flight-demonstrator (visited on 07/19/2024).

[64] Annegret Stephan et al. "Alternative Battery Technologies Roadmap 2030+". In: (2023). Publisher: Fraunhofer ISI. URL: https://publica.fraunhofer.de/handle/publica/451421 (visited on 07/18/2024).

[65] Y Klett. "Design of Multifunctional Folded Core Structures for Aerospace Sandwich Applications". In: (). URL: https://www.fzt.haw-hamburg.de/pers/Scholz/ewade/2007/CEAS2007/papers2007/ceas-2007-253.pdf.

[66] Yide Lin. "The Development and Challenges of More Electric Aircraft". In: *Highlights in Science, Engineering and Technology* 27 (Dec. 27, 2022), pp. 814–819. ISSN: 2791-0210. DOI: 10.54097/hset.v27i.3850. URL: https://drpress.org/ojs/index.php/HSET/article/view/3850 (visited on 07/19/2024).

[67] Maria Coutinho et al. "A review on the recent developments in thermal management systems for hybrid-electric aircraft". In: *Applied Thermal Engineering* 227 (June 5, 2023), p. 120427. ISSN: 1359-4311. DOI: 10.1016/j.applthermaleng.2023.120427. URL: https://www.sciencedirect.com/science/article/pii/S1359431123004568 (visited on 06/17/2024).

[68] Michelangelo Giuliani et al. "Status and Perspectives of Commercial Aircraft Morphing". In: *Biomimetics* 7.1 (Mar. 2022). Number: 1 Publisher: Multidisciplinary Digital Publishing Institute, p. 11. ISSN: 2313-7673. DOI: 10.3390/biomimetics7010011. URL: https://www.mdpi.com/2313-7673/7/1/11 (visited on 07/19/2024).

[69] Vittorio Di Vito et al. *Flight management enabling technologies for single pilot operations in Small Air Transport vehicles in the COAST project*. Oct. 9, 2020.

[70] Miguel Angel Barcala Montejano et al. "Experimental investigation on box-wing configuration for UAS". In: UNMANNED AIR VEHICLE SYSTEMS. INTERNATIONAL CONFERENCE. 26TH. Bristol: E.U.I.T. Aeronáuticos (UPM), Apr. 11, 2011, pp. 1–18. ISBN: 978-1-61839-065-3. URL: http://toc.proceedings.com/12402webtoc.pdf (visited on 07/20/2024).

[71] Mohit Singh et al. "Box Wing: Aerodynamic Experimental Study for Applications in MAVs". In: Feb. 14, 2020. DOI: 10.31219/osf.io/3r79q.

[72] *Electrified Aircraft Propulsion (EAP)*. Glenn Research Center | NASA. URL: https://www1.grc.nasa.gov/aeronautics/eap/ (visited on 07/20/2024).

[73] Burak Tarhan, Ozge Yetik, and Tahir Hikmet Karakoc. "Hybrid battery management system design for electric aircraft". In: *Energy* 234 (Nov. 1, 2021), p. 121227. ISSN: 0360-5442. DOI: 10.1016/j.energy.2021.121227. URL: https://www.sciencedirect.com/science/article/pii/S0360544221014754 (visited on 06/14/2024).

[74] Justin J. Scheidler and Thomas F. Tallerico. "Design, Fabrication, and Critical Current Testing of No-Insulation Superconducting Rotor Coils for NASA's 1.4 MW High-Efficiency Megawatt Motor". In: *2018 AIAA/IEEE Electric Aircraft Technologies Symposium (EATS)*. 2018 AIAA/IEEE Electric Aircraft Technologies Symposium (EATS). July 2018, pp. 1–9. URL: https://ieeexplore.ieee.org/document/8552771 (visited on 07/20/2024).

[75] EUROCAE. *New working group: WG-116 / High Voltage Systems and Components in Aviation*. Eurocae. 2019. URL: https://www.eurocae.net/news/posts/2019/october/new-working-group-wg-116-high-voltage-systems-and-components-in-aviation/ (visited on 07/21/2024).

[76] NICOLA PUCA and GIORGIO GUGLIERI. "Enabling Single-Pilot Operations technological and operative scenarios: a state-of-the-art review with possible cues". In: (2023). Artwork Size: 15 pages Medium: PDF Publisher: Proceedings of the Aerospace Europe Conference - EUCASS - CEAS - 2023, 15 pages. DOI: 10.13009/EUCASS2023-411. URL: https://www.eucass.eu/doi/EUCASS2023-411.pdf (visited on 07/21/2024).